

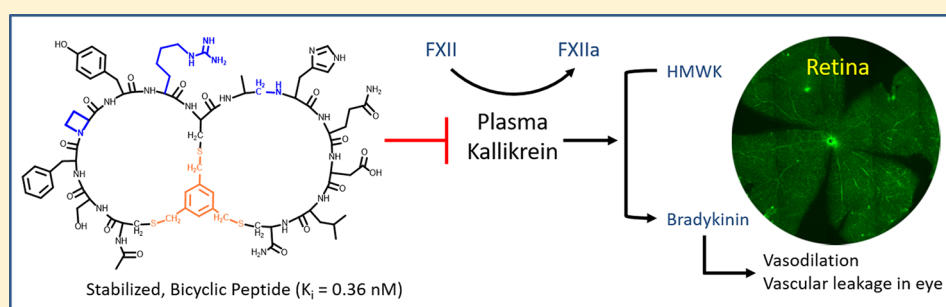
# Stable and Long-Lasting, Novel Bicyclic Peptide Plasma Kallikrein Inhibitors for the Treatment of Diabetic Macular Edema

Daniel P. Teufel,<sup>‡</sup> Gavin Bennett,<sup>‡</sup> Helen Harrison,<sup>‡</sup> Katerine van Rietschoten,<sup>‡</sup> Silvia Pavan,<sup>‡</sup> Catherine Stace,<sup>‡</sup> François Le Floch,<sup>†,‡,‡</sup> Tine Van Bergen,<sup>†,‡</sup> Elke Vermassen,<sup>†</sup> Philippe Barbeaux,<sup>†</sup> Tjing-Tjing Hu,<sup>†</sup> Jean H. M. Feyen,<sup>\*,†</sup> and Marc Vanhove<sup>†</sup> 

<sup>‡</sup>Bicycle Therapeutics Limited, Building 900, Babraham Research Campus, Cambridge CB22 3AT, U.K.

<sup>†</sup>Thrombogenics N.V., Gaston Geenslaan 1, 3001 Leuven, Belgium

## Supporting Information



**ABSTRACT:** Plasma kallikrein, a member of the kallikrein-kinin system, catalyzes the release of the bioactive peptide bradykinin, which induces inflammation, vasodilation, vessel permeability, and pain. Preclinical evidence implicates the activity of plasma kallikrein in diabetic retinopathy, which is a leading cause of visual loss in patients suffering from diabetes mellitus. Employing a technology based on phage-display combined with chemical cyclization, we have identified highly selective bicyclic peptide inhibitors with nano- and picomolar potencies toward plasma kallikrein. Stability in biological matrices was either intrinsic to the peptide or engineered via the introduction of non-natural amino acids and nonpeptidic bonds. The peptides prevented bradykinin release *in vitro*, and *in vivo* efficacy was demonstrated in both a rat paw edema model and in rodent models of diabetes-induced retinal permeability. With a highly extended half-life of ~40 h in rabbit eyes following intravitreal administration, the bicyclic peptides are promising novel agents for the treatment of diabetic retinopathy and diabetic macular edema.

## ■ INTRODUCTION

Plasma kallikrein (PKal) is a serine protease present in blood plasma at a relatively high concentration (30–50  $\mu\text{g}/\text{mL}$ )<sup>1,2</sup> in the form of the inactive zymogen prekallikrein. PKal is positioned at the interface between the contact activation system (CAS) and the kallikrein-kinin system (KKS). Within the CAS, PKal is involved in a reciprocal activation loop with the coagulation factor XII (Factor XII) leading to activation of the coagulation factor XI (Factor XI) and eventually activation of the intrinsic blood coagulation pathway. Within the KKS, PKal activity releases the nonapeptide bradykinin (BK) from the high molecular weight kininogen (HMWK). BK then signals through the constitutive bradykinin B2 G-protein-coupled receptor and, via its des-Arg<sub>7</sub> metabolite, through the inducible bradykinin B1 G-protein-coupled receptor, leading to the production of mediators of inflammation, angiogenesis, vasodilation, increased vessel permeability, and pain.<sup>3,4</sup> Unlike in the CAS, where conversion of the inactive zymogen prekallikrein into active PKal is mediated by Factor XIIa, conversion of the zymogen in the KKS system can occur both in a Factor XIIa-dependent and -independent manner.<sup>5,6</sup>

*In vivo*, active PKal is mostly controlled by the serpin family derived C1 inhibitor (C1-INH), whose genetic deficiency or dysfunction causes hereditary angioedema (HAE). HAE is a rare, autosomal dominant disorder that clinically manifests as episodic attacks of subcutaneous or mucosal edema of the face, upper respiratory and gastrointestinal tracts, limbs, or genitalia.<sup>7</sup> Therapies to treat and prevent HAE attacks include treatment with plasma-derived or recombinant C1-INH, the PKal inhibitor drug Ecallantide, or the B2 receptor antagonist Icatibant.<sup>8,9</sup>

Diabetic retinopathy (DR) is one of the most prevalent complications of diabetes mellitus and a leading cause of vision loss in industrialized countries.<sup>10–13</sup> Clinical manifestations of DR represent different stages that can be classified as nonproliferative diabetic retinopathy (NPDR) and proliferative diabetic retinopathy (PDR). Diabetic macular edema (DME) represents the major cause of moderate to severe visual loss in NPDR or PDR.<sup>14</sup> It is estimated that the population of diabetic

Received: November 14, 2017

Published: March 8, 2018

patients worldwide will grow from 285 million in 2010 to 439 million by 2030, and the DR patient population is expected to grow in parallel.<sup>15</sup> By 2030, the number of DR patients and of patients with vision-threatening DR has been projected to rise to 191 million and 56.3 million, respectively.<sup>16</sup> Current treatments for DR or DME include laser photocoagulation, steroidal or nonsteroidal anti-inflammatory drugs, anti-VEGF agents, and vitrectomy.<sup>14,17</sup>

More recently, experimental and clinical data have also implicated the KKS in DR development.<sup>18</sup> For example, the level of components of the KKS system, including PKal, was shown to be increased both in diabetic animal models and in the vitreous of diabetic patients.<sup>19–22</sup> Furthermore, both PKal and BK have been reported to induce retinal vascular permeability (RVP) in animal models,<sup>19,23</sup> while inhibition by either PKal inhibitors or B1/B2 receptors antagonists improved diabetes-induced retinal dysfunction in rat models.<sup>19,23–25</sup> Finally, RVP in diabetic, PKal knockout mice was observed to be reduced compared to diabetic wild-type animals.<sup>22</sup> This prompted the investigation of alternative therapeutic approaches, one of which is using direct PKal inhibition with the small molecule inhibitor KVD001 (Kalvista Pharmaceuticals), which has completed its first-in-human study in patients with DME and is being prepared for Phase 2.<sup>14</sup>

In light of the strong evidence for the involvement of PKal in the development of DR and DME, we sought to develop new therapeutic modalities for its effective treatment. Here, we describe the identification, molecular optimization, and *in vitro/in vivo* characterization of a series of highly potent, stable, and long-lasting PKal inhibitory bicyclic peptides. Bicyclic peptides (Figure 1A) are more constrained than either conventional linear or monocyclic peptides, allowing them to exhibit properties (e.g., affinity and target specificity) that are more generally associated with antibodies.<sup>26,27</sup> PKal inhibitory activity of these peptides was demonstrated in a variety of *in vitro* assays and in a variety of biological matrices, and *in vivo* efficacy was demonstrated in both a rat paw edema model and in rodent models of diabetes-induced retinal permeability. The data presented here demonstrate that bicyclic constrained peptides act as potent and highly specific PKal inhibitors with therapeutic potential to targeting plasma kallikrein-mediated conditions of edema.

## RESULTS

**Discovery of Anti-plasma Kallikrein Bicyclic Peptides by Phage Display and Chemical Optimization.** Bicyclic peptides consist of a peptide sequence containing 3 cysteine residues, which are covalently linked to a thiol-reactive molecular scaffold. A number of thiol-reactive scaffolds are available,<sup>28</sup> and in this instance, we chose 1,3,5-tris-(bromomethyl)benzene (TBMB) (Figure 1A). Using large phage libraries of linear peptides containing 3 invariant cysteines that are cyclized *in situ* to form thioether-bonded bicyclic peptide libraries, selections and subsequent affinity maturation selections were performed against PKal using methodology described previously.<sup>26,29</sup> Rat and human PKal orthologous enzymes were alternated as baits during each selection round in order to identify bicyclic peptides with good cross-reactivity that would facilitate their study in preclinical animal models.

**Bicyclic Peptide 1b.** A promising sequence output was peptide 1a, of sequence AC<sub>i</sub>NTWNPWC<sub>ii</sub>PWDAPLC<sub>iii</sub>A. Using enzyme inhibition assays, this peptide showed strong

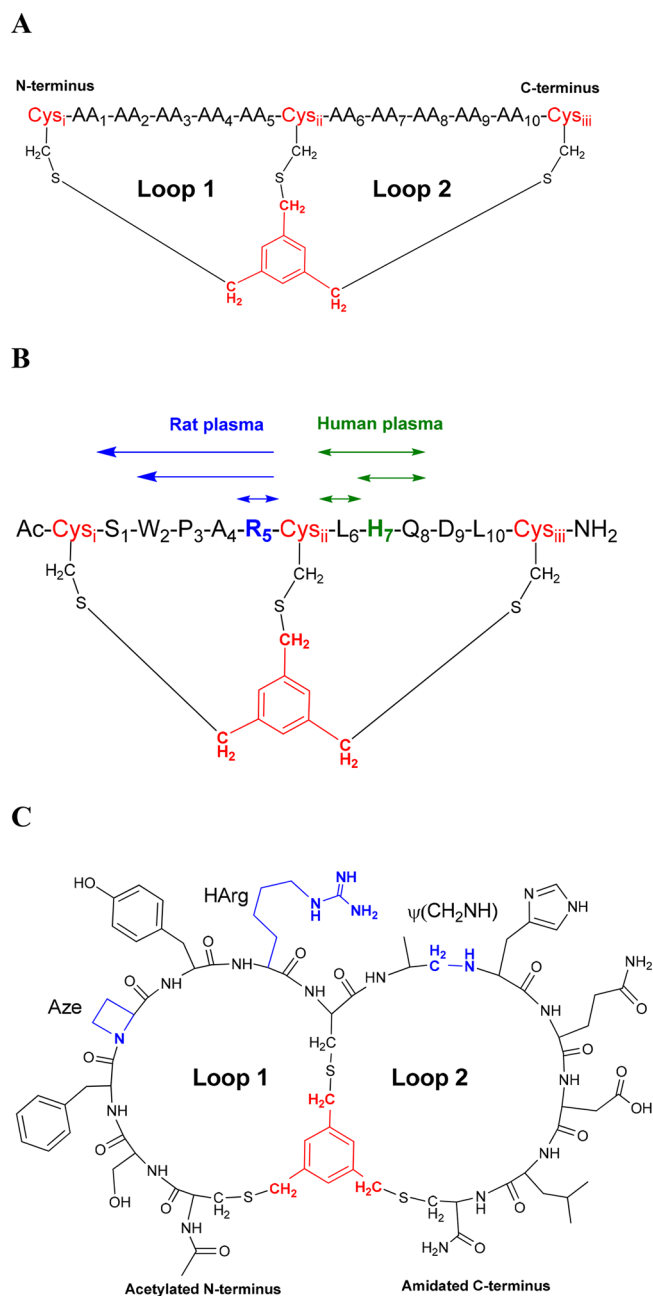


**Figure 1.** Structure of bicyclic peptides. (A) Canonical structure of bicyclic peptides containing 5 AA in each loop (5 × 5). Any loop format is possible, referred to in text as 6 × 6 and 5 × 6 bicyclic peptides. Cysteine residues and the 1,3,5-trimethylbenzene scaffold are indicated in red. Loop 1 is located between Cys<sub>i</sub> and Cys<sub>iii</sub>, Loop 2 is located between Cys<sub>ii</sub> and Cys<sub>iii</sub>. Residue numbering begins following the N-terminal first Cys<sub>i</sub>. (B) Rat and human plasma protease activity on 2b. Rat and human cleavage sites and successive excision of peptide segments are indicated in blue and green, respectively. (C) Chemical structure of 2d. The central scaffold is shown in red, with non-natural modifications (Aze, HArg, pseudopeptide bond) indicated in blue. All amino acids are in their L-configuration.

inhibitory activity to both human and rat PKal ( $K_i = 2.3 \pm 2.7$  and  $0.40 \pm 0.24$  nM, respectively). Qualitative stability assessment using a matrix-assisted laser desorption ionization time-of-flight (MALDI-TOF) assay in rat plasma revealed rapid removal of the N/C-terminal alanine residues which are

Table 1.  $K_i$  Values (nM) against PKal from Various Species<sup>a</sup>

PKal species	1b	2b	2c	2d	4b
human	3.0 ± 0.3	0.15 ± 0.18	0.39 ± 0.17	0.36 ± 0.07	0.25 ± 0.20
cynomolgus	3.1 ± 0.1	n.d.	n.d.	2.7 ± 0.5	0.86 ± 0.13
mouse	54 ± 4	n.d.	n.d.	120 ± 20	45 ± 6
rat	3.4 ± 1.1	2.0 ± 0.9	11 ± 4	30 ± 9	5.5 ± 3.8
rabbit	~1,450	10 ± 2	84 ± 24	3,400 ± 200	~2,650
pig	410 ± 30	3.6 ± 0.6	22 ± 3	510 ± 60	300 ± 10
dog	500 ± 90	n.d.	n.d.	80 ± 10	22 ± 3

<sup>a</sup>n.d. not determined. Errors are expressed as standard deviation.

situated outside the loop structures. Furthermore, the peptide displayed poor solubility in aqueous buffers, and consequently a derivative, termed **1b**, was synthesized that replaced the N-terminal Ala with an acetyl group and that contained a C-terminal extension following the C-terminal alanine composed of 3 sarcosines and 2 D-arginine residues (sequence Ac-C<sub>1</sub>NTWNPWC<sub>ii</sub>PWDAPLC<sub>iii</sub>A-Sar<sub>3</sub>-[D-Arg]<sub>2</sub>). The former is a benign molecular spacer with good aqueous solubility properties,<sup>30</sup> and the latter imparts higher aqueous solubility to the molecule due to the strongly ionic, water-complexing nature of the guanidiny groups at physiological pH. D-Arginine residues were chosen rather than L-arginine residues to render these amino acids (AA) resistant to proteolytic removal.<sup>31</sup>

**1b** showed adequate solubility in aqueous buffers and retained overall potency and good cross-reactivity to both rat and human PKal (Table 1). Furthermore, the peptide was stable in blood plasma derived from three species (Table 2), with no measurable degradation occurring over 24 h.

Table 2. *In Vitro* Stability (Expressed As Half-Life) of Bicyclic Peptides in Vitreous Humor and Plasma

species	matrix	1b	2d	2b
human	vitreous	>24 h	>24 h	>24 h
mouse	plasma	>24 h	>24 h	1.5 h
rat	plasma	>24 h	>24 h	2.8 h
human	plasma	>24 h	>24 h	7 h

**2b** and Chemically Optimized **2d**. Using 5 × 5 phage libraries, one of the sequence outputs termed **2a** (sequence: AC<sub>i</sub>SWPARC<sub>ii</sub>LHQDLC<sub>iii</sub>A) showed high potency to human and rat PKal ( $K_i = 0.07 ± 0.02$  and  $0.90 ± 0.33$  nM, respectively). A variant was synthesized lacking the protease labile terminal alanine residues (**2b**, sequence Acetyl-C<sub>i</sub>S<sub>1</sub>W<sub>2</sub>P<sub>3</sub>A<sub>4</sub>R<sub>5</sub>C<sub>ii</sub>L<sub>6</sub>H<sub>7</sub>Q<sub>8</sub>D<sub>9</sub>L<sub>10</sub>C<sub>iii</sub>), and its potency toward both rat and human PKal was retained (Table 1). However, the plasma stability of **2b** was poor, with a half-life of 1.5 h, 2.8 h, and 7 h in mouse, rat, and human plasma, respectively (Table 2). MALDI-TOF analysis of the peptide exposed to rat plasma revealed endoproteolytic loop opening and exoproteolytic removal of Arg<sub>5</sub> in Loop 1, followed by removal of all residues in Loop 1 (Figure 2A). By contrast, exposure to human plasma revealed Loop 2 opening followed by removal of 3 fragments (L<sub>6</sub>H<sub>7</sub>Q<sub>8</sub>, H<sub>7</sub>Q<sub>8</sub>, L<sub>6</sub>) (Figure 2B). The initial endoproteolytic event appeared to occur on the N- or C-terminal side of His<sub>7</sub>. Thus, **2b** appears to contain two sites (Arg<sub>5</sub> and His<sub>7</sub>) that render the molecule sensitive to proteolytic attack by rat and human plasma proteases (Figure 1B), respectively, with the consequence that this molecule is likely not sufficiently stable for *in vivo* studies.

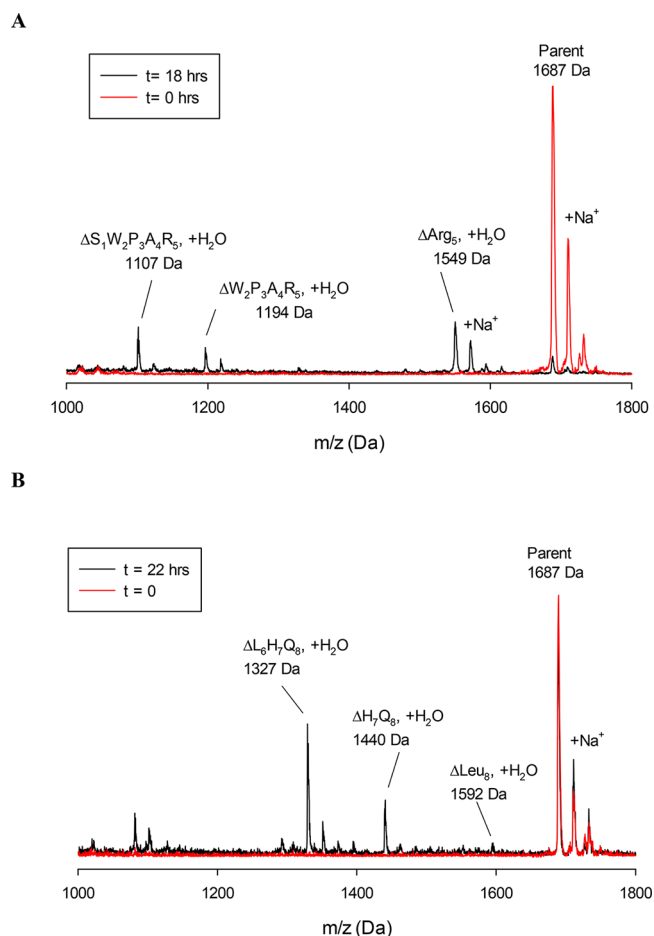


**Figure 2.** Degradation of bicyclic peptide **2b** in plasma. (A) MALDI-TOF derived ion chromatograms of **2b** exposed to rat plasma. Removal of Arg<sub>5</sub> in Loop 1 is observed, with larger fragments being excised subsequently. Note the low signal for intact parent peptide following 18 h of incubation. (B) MALDI-TOF derived ion chromatograms of **2b** exposed to human plasma. Removal of 3 fragments in Loop 2 is observed, centering on His<sub>7</sub>.

We undertook a campaign of chemical derivatization of **2b** to identify variants with enhanced stability toward plasma proteases, while maintaining the potency and specificity profile. Structure activity relationships were assessed by performing partial alanine and D-AA scans in each loop to assess the energetic role of each AA side chain in binding, and to assess the steric requirement of side chain projection on binding, respectively. Furthermore, the derivatives were assessed for changes in proteolytic cleavage patterns in rat/human plasma using MALDI-TOF.

In Loop 1, D-amino acid replacement reduced affinities to 50 nM and beyond. However, it is of interest that D-AA replacement at positions 4 and 5 markedly reduced Loop 1 degradation by rat plasma, in that no des-Arg fragments could be detected. Consequently, a variety of arginine isosteres were tested at position 5 in Loop 1 (including citrulline,  $\alpha$ -N-methyl arginine, 4-guanidino-phenylalanine, Arg side chain length variants homoarginine (C4), beta-homoarginine, and the shorter side chain derivatives 2-amino-4-guanidinobutyric (C2) and 2-amino-3-guanidinopropionic acid (C1)). Strikingly, all isosteres reduced Loop 1 degradation by rat plasma. Homoarginine at position 5 (HArg<sub>5</sub>) and  $\alpha$ -N-methyl Arg<sub>5</sub> derivatives retained potencies at 2.1 and 3.5 nM (however still 10–20-fold lower than the parent molecule, Table 3).

**Table 3. Summary of Chemical Modifications and Comparative  $K_i$  Values (nM) for Human PKal during the Optimization Campaign of 2b To Produce the Highly Stabilized Derivative 2d<sup>a</sup>**

family	substitutions	$K_i$ (nM)	protection of Loop 1 and/or Loop 2
2b	parent compound, no modifications	0.15 ± 0.18	none
	Arg <sub>5</sub> → HArg <sub>5</sub>	2.1 ± 2.6	Loop 1
	Pro <sub>3</sub> → Aze <sub>3</sub>	0.06 ± 0.01	none
	Pro <sub>3</sub> → Aze <sub>3</sub> , Arg <sub>5</sub> → HArg <sub>5</sub>	0.14 ± 0.02	Loop 1
2c	Trp <sub>2</sub> → Phe <sub>2</sub> , Ala <sub>4</sub> → Tyr <sub>4</sub>	0.39 ± 0.17	none
	Trp <sub>2</sub> → Phe <sub>2</sub> , Pro <sub>3</sub> → Aze <sub>3</sub> , Ala <sub>4</sub> → Tyr <sub>4</sub> , Arg <sub>5</sub> → HArg <sub>5</sub>	0.21 ± 0.15	Loop 1
	Trp <sub>2</sub> → Phe <sub>2</sub> , Ala <sub>4</sub> → Tyr <sub>4</sub> , Leu <sub>6</sub> → Ala( $\psi$ CH <sub>2</sub> NH) <sub>6</sub>	1.3 ± 0.3	Loop 2
2d	Trp <sub>2</sub> → Phe <sub>2</sub> , Pro <sub>3</sub> → Aze <sub>3</sub> , Ala <sub>4</sub> → Tyr <sub>4</sub> , Arg <sub>5</sub> → HArg <sub>5</sub> , Leu <sub>6</sub> → Ala( $\psi$ CH <sub>2</sub> NH) <sub>6</sub>	0.36 ± 0.07	Loop 1 and Loop 2

<sup>a</sup>Errors are expressed as standard deviation.

Further isostere substitution was conducted at proline 3. Proline is a secondary AA, containing the alpha nitrogen within a 5-membered ring structure. The isosteres azetidine-carboxylic acid (4-membered ring, Aze) and pipercolic acid (6-membered ring structure, Pip) were incorporated and tested for potency. Unexpectedly, replacement with Aze increased the potency to  $K_i = 0.06$  nM (compared to 0.15 nM for parent), while Pip lowered the potency slightly ( $K_i = 0.26$  nM). The fragmentation of Loop 1 in the presence of rat plasma remained unchanged. Taking the two modifications together, i.e. the affinity enhancing Pro<sub>3</sub> → Aze<sub>3</sub> and stability enhancing Arg<sub>5</sub> → HArg<sub>5</sub> replacements, produced a bicyclic peptide with fully retained potency to human PKal at  $K_i = 0.14$  nM (Table 3) and with enhanced stability of Loop 1 in rat plasma.

Next, we returned to a derivative of 2b containing two changes (W<sub>2</sub> → F<sub>2</sub> and A<sub>4</sub> → Y<sub>4</sub>, termed 2c, of sequence Ac-C<sub>1</sub>S<sub>1</sub>F<sub>2</sub>P<sub>3</sub>Y<sub>4</sub>R<sub>5</sub>C<sub>ii</sub>L<sub>6</sub>H<sub>7</sub>Q<sub>8</sub>D<sub>9</sub>L<sub>10</sub>C<sub>iii</sub>). This sequence, which was derived from phage selections, was of interest due to the replacement of the oxidation-labile Trp<sub>2</sub> with tyrosine. The affinity of this derivative was virtually unchanged, and likewise, incorporating Pro<sub>3</sub> → Aze<sub>3</sub> and Arg<sub>5</sub> → HArg<sub>5</sub> substitutions yielded a fully potent, but Loop 1-stabilized, tryptophan-deficient Bicycle (Table 3).

Finally, efforts focused on the stabilization of Loop 2, where His<sub>7</sub> is the recognition point for human plasma proteases. The alanine scan in Loop 2 (using 2c) did not dramatically lower potencies, with  $K_i$ 's not increasing beyond 23.4 nM for H<sub>7</sub> →

A<sub>7</sub>. Interestingly, removal of the His<sub>7</sub> side chain reduced Loop 2 degradation in human plasma, confirming the role of this residue in providing a recognition point for human plasma proteases. Both D-AA and D-alanine replacement in Loop 2 at or near His<sub>7</sub> produced peptide derivatives with enhanced stability, however at the cost of markedly reduced affinity (data not shown). A range of histidine isosteres, probing requirement of charge, molecular shape, and/or aromaticity of the histidine side chain, invariably produced molecules with lower potency. Consequently, we investigated whether AA backbone changes, which potentially render the molecule stable to proteolytic hydrolysis, were tolerated.  $\alpha$ -N-Methylation of Leu<sub>6</sub>, His<sub>7</sub>, or Gln<sub>8</sub>, rendered the molecule stable to human plasma, but  $K_i$ 's were >50 nM. In an attempt to modify the peptide backbone itself, a reduced form of the peptide bond was introduced between Leu<sub>6</sub> and His<sub>7</sub>. Here, Leu<sub>6</sub> was replaced by Ala<sub>6</sub>, and the carbonyl on this residue was reduced to methylene, yielding a pseudo peptide bond ( $\psi$ CH<sub>2</sub>-NH versus CO-NH). Due to the absence of the hydrolyzable peptide bond, the peptide was stable in human plasma as Loop 2 fragmentation could not be observed, and potency was high (Table 3). Introduction of Ala( $\psi$ CH<sub>2</sub>-NH)<sub>6</sub> in the context of the previously described stability and potency-enhancing modifications in Loop 1 (Phe<sub>2</sub>, Aze<sub>3</sub>, Tyr<sub>4</sub>, HArg<sub>5</sub>) produced a candidate molecule (2d, Figure 1C) which showed, using quantitative stability measurement in human, rat, or mouse plasma, no measurable degradation (Table 2, Supporting Information Figure 1 and Table 1). With a potency of 0.36 nM (Table 1 and 3), 2d presents an attractive molecule for further study and demonstrates a stark improvement over the original parent compound 2b in terms of stability.

**Bicyclic Peptide 4b.** Phage selections further identified a 6 × 6 peptide of sequence AC<sub>i</sub>N<sub>ii</sub>N<sub>ii</sub>FP<sub>ii</sub>FC<sub>ii</sub>VYYPD<sub>iii</sub>A (termed 3) that had a high potency ( $K_i = 0.44 \pm 0.07$  nM) to human PKal. Of note, this peptide comprises the FPF<sub>ii</sub> motif in Loop 1, which is similar to the WPAR and FPYR motif described previously for the peptide 2 family. Importantly, the equivalent His<sub>7</sub> proteolytic recognition site in Loop 2 is absent, rendering this loop potentially stable without chemical modification. Given the similarity of Loop 1 of 3 with Loop 1 of the peptide 2 family, we reasoned that 2c could be used as a template where its His<sub>7</sub>-containing Loop 2 is replaced with Loop 2 from 3, generating a chimeric bicyclic peptide of sequence AC<sub>i</sub>SFP<sub>ii</sub>YRC<sub>ii</sub>VYYPD<sub>iii</sub>A (termed 4a). Note the asymmetry of the loop sizes: 5 AA in Loop 1 and 6 AA in Loop 2. 4a still contains the Arg<sub>5</sub> protease recognition point, thus the chemically stabilized variant containing Aze<sub>3</sub> and HArg<sub>5</sub> was generated, following findings described above. This bicyclic peptide however displayed poor aqueous solubility, and consequently the final derivative 4b (sequence Ac-C<sub>1</sub>SF[Aze]Y[HArg]C<sub>ii</sub>VYYPD<sub>iii</sub>A-Sar<sub>3</sub>-[D-Arg]<sub>2</sub>) was generated containing the solubilizing Sar<sub>3</sub>-[D-Arg]<sub>2</sub> extension described earlier. The potency was high, at  $K_i = 0.27 \pm 0.22$  nM (Table 1).

#### Inhibitory Properties and Species Cross-Reactivity.

The inhibitory activity of the bicyclic peptides was assessed via  $K_i$  determination in enzyme inhibition assays. Control measurements using aprotinin, an antifibrinolytic proteinaceous drug with well-characterized inhibitory activity toward PKal, trypsin, chymotrypsin, plasmin, thrombin, and activated protein C,<sup>32</sup> were performed with the objective of validating the potencies of the PKal-inhibiting bicyclic peptides. Our assay using aprotinin ( $K_i$  at 27 nM to human PKal) showed excellent correlation with published data (30 nM to human PKal).<sup>33</sup>

All tested peptides proved to be highly potent (single-digit nanomolar or subnanomolar) inhibitors of human PKal (Table 1), with a representative example shown in Figure 3. Robust

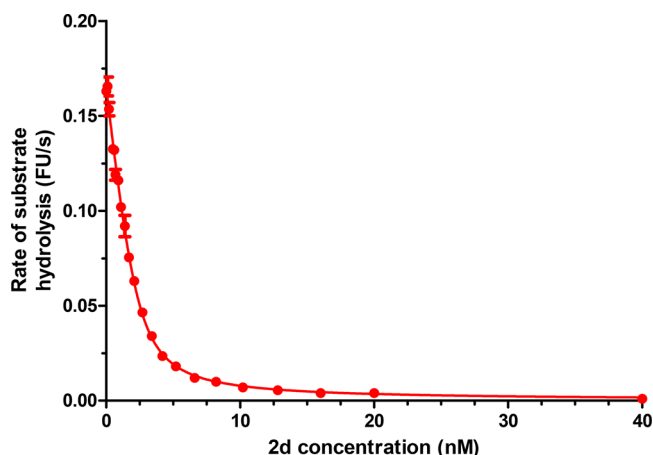


**Figure 3.** Inhibition of human PKal activity by the bicyclic peptide **2d**. Each data point represents the mean  $\pm$  SD of duplicate measurements. The solid line represents the best fit obtained using eq 1.

cross-reactivity toward cynomolgus PKal was observed, at least for the three tested peptides (namely **1b**, **2d**, and **4b**), which was expected given the high degree of identity (95%) between the human and cynomolgus PKal sequences. The cross-reactivity of the same three peptides was also found to be relatively strong against rat PKal, but weaker against the mouse, dog, or pig enzymes, and poor against the rabbit enzyme (identity between the human PKal sequence and the sequences of rat, mouse, dog, pig, and rabbit PKal is 75, 76, 82, 80, and 82%, respectively).

**Specificity against a Panel of Proteases.** The specificity of the **1b**, **2d**, and **4b** peptides, which represent the most stable, soluble, and potent members of peptide sequence families 1, 2, and 4, was assessed by measuring their ability to inhibit a variety of serine proteases (Table 4). We found that **1b** and **2d** are highly specific, none of the tested proteases being inhibited

**Table 4.**  $K_i$  for the **1b**, **2d**, and **4b** Peptides against a Panel of Human Serine Proteases

protease	<b>1b</b>	<b>2d</b>	<b>4b</b>
KLK1	>50 $\mu$ M	>50 $\mu$ M	$\sim$ 50 $\mu$ M
KLK2	>50 $\mu$ M	$\sim$ 10 $\mu$ M	$\sim$ 10 $\mu$ M
KLK5	$\sim$ 50 $\mu$ M	>50 $\mu$ M	0.8 $\mu$ M
KLK6	>50 $\mu$ M	>50 $\mu$ M	>50 $\mu$ M
KLK12	>50 $\mu$ M	>50 $\mu$ M	>50 $\mu$ M
KLK13	>50 $\mu$ M	>50 $\mu$ M	0.82 $\mu$ M
KLK14	>50 $\mu$ M	>50 $\mu$ M	$\sim$ 2 $\mu$ M
Plasmin	>50 $\mu$ M	>50 $\mu$ M	>50 $\mu$ M
Alpha thrombin (Factor IIa)	>50 $\mu$ M	>50 $\mu$ M	>50 $\mu$ M
Factor VIIa	>50 $\mu$ M	>50 $\mu$ M	>50 $\mu$ M
Factor Xa	>50 $\mu$ M	>50 $\mu$ M	$\sim$ 23 $\mu$ M
Factor XIa	>50 $\mu$ M	>50 $\mu$ M	0.5 $\mu$ M
Factor XIIa	>50 $\mu$ M	>50 $\mu$ M	>50 $\mu$ M
Activated protein C	>50 $\mu$ M	>50 $\mu$ M	>50 $\mu$ M
Matriptase	$\sim$ 40 $\mu$ M	$\sim$ 50 $\mu$ M	$\sim$ 15 $\mu$ M
Complement component C 1s	>50 $\mu$ M	>50 $\mu$ M	>50 $\mu$ M
Granzyme B	>50 $\mu$ M	>50 $\mu$ M	>50 $\mu$ M
Cathepsin G	>50 $\mu$ M	>50 $\mu$ M	>50 $\mu$ M

with a  $K_i$  value lower than 10  $\mu$ M. The selectivity profile of **4b** was slightly less specific, with four proteases inhibited with  $K_i$  values in the 1–2  $\mu$ M range (KLK5, KLK13, KLK14, and Factor XIa). Of note, none of the tested peptides was able to inhibit Factor XIIa, which is the main physiological activator of prekallikrein, and therefore these peptides are not expected to interfere with prekallikrein activation.

**Activity in aPTT Assay.** Prekallikrein, together with the HMWK, Factor XI, and Factor XII, is part of the contact activation system, a group of circulating proteins that responds to the presence of (patho)physiological materials and invasion pathogens. Factor XII, once activated by surface contact to active Factor XIIa, catalyzes the conversion of prekallikrein into active PKal which in turn catalyzes further Factor XII to XIIa conversion (where the latter activates Factor XI). This generates an activation feedback loop that overcomes inactivation of PKal and Factor XIIa by their natural inhibitors<sup>34</sup> that subsequently leads to onset of coagulation.

Previous work demonstrated that kunitz-domain inhibitors of PKal were able to reduce clotting times 3.5-fold, using the activated partial thromboplastin time (aPTT) assay that measures the activity of the intrinsic and common pathways of coagulation.<sup>35</sup> For this reason, we were interested in testing the most promising PKal targeting peptides **1b**, **2d**, and **4b** in the aPTT assay using human plasma (Figure 4). Surprisingly,

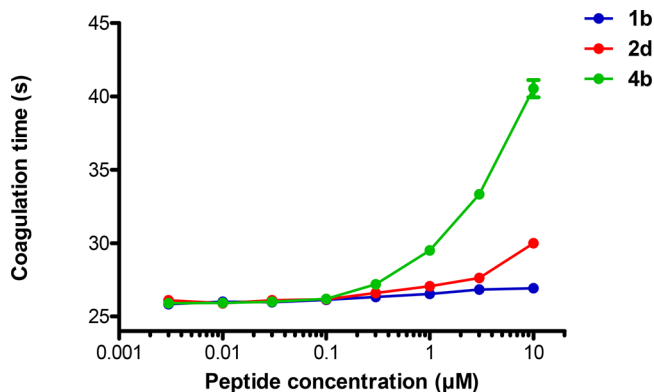


**Figure 4.** Effect of **1b**, **2d**, and **4b** on the coagulation time in the aPTT assay. Each data point represents the mean  $\pm$  SD of triplicate measurements.

**1b** and **2d** induced only a limited increase in coagulation time in this assay (less than 5% and  $\sim$ 15% for **1b** and **2d**, respectively, at 10  $\mu$ M). By contrast, although remaining close to the normal range of 26 to 40 s,<sup>36</sup> the coagulation time increased  $\sim$ 1.5-fold in the presence of 10  $\mu$ M of **4b**, which may reflect the slightly lower selective profile of the molecule, in particular for Factor XIa (Table 4). Together, these data led us to select **1b** and **2d** for further characterization.

**Stability in Vitreous Humor.** Both **1b** and **2d** were tested for stability in human vitreous in addition to nonstabilized **2b** as a comparator. All three tested peptides were highly stable (half-lives >24 h) in human vitreous, including the plasma-sensitive **2b** peptide (Table 2). The latter finding is likely to reflect the relatively low protein/protease content in vitreous (<1%).<sup>37</sup>

**Inhibition of Bradykinin Release in Plasma.**  $K_i$  measurements as those described above are important to determine the intrinsic potency (i.e., the affinity) of inhibitory peptides toward PKal. However, they do not demonstrate the ability of such peptides to block the activity of PKal against its

natural substrate, i.e. HMWK. We therefore developed an assay in plasma where active PKal is generated from the endogenous pool of prekallikrein upon addition of kaolin, and where activity on HMWK is monitored through the quantification of released BK using ELISA. Kaolin, also known as kaolinite, is a clay mineral of chemical composition  $\text{Al}_2\text{Si}_2\text{O}_5(\text{OH})_4$  which here acts as an activator of the contact phase of the coagulation pathway. **2d** was able to inhibit BK release in a dose-dependent manner, with an  $\text{IC}_{50}$  of  $120 \pm 60$  nM. A typical example of inhibition of BK production in human plasma is shown in Figure 5. **1b**, also tested in the same assay, proved slightly less

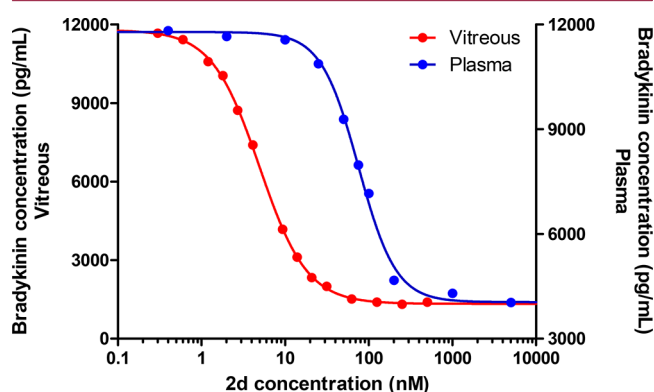


**Figure 5.** Inhibition of bradykinin release in plasma and vitreous by **2d**. Each data point represents a single measurement. The solid lines represent the best fits obtained using eq 3. The left and right Y-axes represent the bradykinin concentration in the vitreous and in plasma, respectively.

potent ( $\text{IC}_{50} = 790 \pm 220$  nM). It should be noted here that the difference between the  $K_i$  values reported in Table 1 and the  $\text{IC}_{50}$  values measured here is most likely due to the fact that the PKal concentration produced by kaolin-induced conversion from prekallikrein is very high (prekallikrein concentration in blood plasma is  $30\text{--}50$   $\mu\text{g}/\text{mL}$ ),<sup>1,2</sup> which requires at least several times this concentration of inhibitory peptides to effectively inhibit all PKal activity and associated BK production.

In a similar assay performed in rabbit plasma instead of human plasma, **2d** was unable to block BK release even at a concentration of  $2$   $\mu\text{M}$  (data not shown), which is explained by its poor cross-reactivity toward the rabbit enzyme (see Table 1). Together, provided cross-reactivity to PKal is maintained, both peptides can effectively block PKal in blood plasma, leading to concomitant suppression of downstream BK production.

**Inhibition of Bradykinin Release in Vitreous.** Given that intravitreal (IVT) injection is a potential route of administration for therapeutic PKal inhibitory peptides in the context of diabetic eye diseases, we also tested the ability of the peptides to block PKal activity on HMWK in vitreous. Unlike plasma, vitreous does not contain PKal or HMWK at high concentrations, and therefore an assay where purified reagents were spiked into vitreous was used (see the Experimental Section). Both **2d** and **1b** were shown to block BK release in this assay, although here **2d** also proved slightly superior to **1b** ( $\text{IC}_{50} = 6.0 \pm 0.9$  and  $27 \pm 18$  nM, respectively). A representative data set is shown in Figure 5. Due to the lower, defined concentration of PKal ( $10$  nM) that was spiked

into vitreous, the resulting  $\text{IC}_{50}$ s for both peptides are lower than those observed in plasma above.

**Pharmacokinetics Following Intravenous Administration.** Evaluation of plasma pharmacokinetics following intravenous dosing in rats showed a profile consistent with that expected of a small peptide construct and with the plasma stabilities shown above. For both **2d** and **1b**, clearances were moderate, consistent with renal clearance at glomerular filtration rate.<sup>38</sup> Peptide **2d** showed a low volume of distribution ( $0.44$  L/kg), with **1b** having a slightly higher volume ( $0.93$  L/kg). This led to plasma half-lives of  $\sim 48$  min (**2d**) and  $\sim 78$  min (**1b**) (Table 5).

**Table 5.** Pharmacokinetic Parameters Following Intravenous Dosing in Rat<sup>a</sup>

parameter	<b>1b</b>	<b>2d</b>	<b>2b</b>
$t_{1/2}$ (min)	78	48	n.d.
Clp (mL/min/kg)	8.2	6.2	156
Vdss (L/kg)	0.93	0.44	n.d.

<sup>a</sup>n.d. not determined.

For peptide **2b**, a markedly higher clearance was observed in the *in vivo* rat. Plasma exposure was measurable during infusion but not following the end of infusion. Clearance was very high (estimated  $\sim 150$  mL/min/kg) (Table 5). The high clearance rate is likely due to the fast degradation of the peptide by plasma proteases *in vivo* and is not unexpected given the poor stability of the peptide in *ex vivo* blood plasma (Table 2).

**Pharmacokinetics Following Intravitreal Administration.** Rabbit was selected as an animal model for intravitreal pharmacokinetics because of its relevance and predictability for translation into intravitreal pharmacokinetics in human.<sup>39</sup> Following IVT administration to rabbits, **2d** showed a long residence time in the eye, with a half-life of  $39 \pm 2$  h (Figure 6).

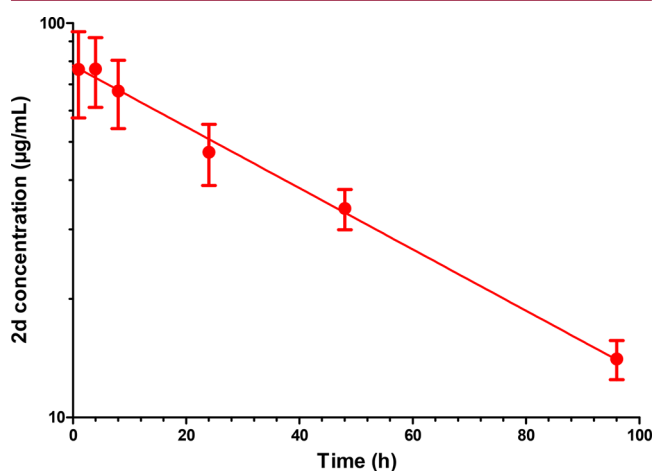


**Figure 6.** Vitreous concentrations of the **2d** peptide following intravitreal administration in rabbit. Calculated half-life is  $39 \pm 2$  h.

In a similar study, **4b** showed a slightly faster clearance, with a half-life of  $\sim 22$  h (data not shown). Furthermore, when either of these two peptides was injected in only one eye, the peptide levels in the contralateral eye as well as in plasma were found to be below the lower limit of detection of the LC-MS/MS method described in the Experimental Section, i.e.  $1$  ng/mL in vitreous and  $2.8$  ng/mL in plasma.

The concentration of peptide **2d** as reported in Figure 6 decreased from  $\sim 45 \mu\text{M}$  ( $\sim 76 \mu\text{g}/\text{mL}$ ) at the earliest time points down to  $\sim 8 \mu\text{M}$  ( $\sim 14 \mu\text{g}/\text{mL}$ ) at the latest time point. Despite the poor potency of **2d** against rabbit PKal ( $K_i = 3400 \text{ nM}$ , Table 1), endogenous PKal inhibition would be predicted to exceed 90% at the earliest time points and would still be  $\sim 70\%$  at the latest time point. Importantly, similar peptide concentrations in the human eye would result in a virtually complete inhibition of human PKal.

**Efficacy in a Rat Paw Edema Model.** The *in vivo* efficacy of **2d** and **1b** was investigated in a rat model of carrageenan-induced paw edema. This animal model is often used to study acute inflammation-induced edema formation and exhibits a pronounced therapeutic window, which enables dose response profiling. In response to carrageenan injection, the vehicle control group developed a distinct increase in paw volume, which peaked at 4 h (Figure 7A). Fifteen-minute pretreatment

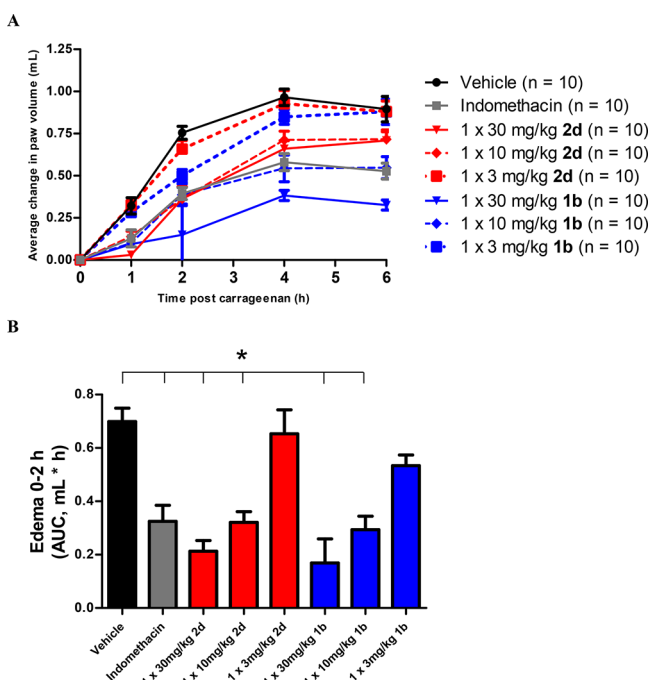


**Figure 7.** *In vivo* efficacy of **2d** and **1b** in a male, Sprague-Dawley rat paw edema model. (A) Subplantar carrageenan injection induced a distinct increase in paw volume in the vehicle control group. Pretreatment with the positive control indomethacin via IP injection (5 mg/kg) resulted in a significant inhibition of the carrageenan-induced paw edema. Pretreatment with IP injection (30, 10, or 3 mg/kg) of **1b** or **2d** resulted in a significant and dose-dependent inhibition of the carrageenan-induced response. (B) The area under the curve was calculated for the different conditions from 0 to 2 h, which revealed a prominent dose-response for both **2d** and **1b**. Data are shown as mean  $\pm$  SEM (\*  $p < 0.05$ ).

with intraperitoneal (IP) injection of either **1b** or **2d** resulted in a significant and dose-dependent inhibition of the carrageenan-induced paw edema (Figure 7A). At the highest dose (30 mg/kg), **1b** significantly reduced paw edema at 1 h (71%), 2 h (59%), 4 h (60%), and 6 h (64%) following carrageenan administration. The highest dose of **2d** (30 mg/kg) resulted in a significant inhibition of the carrageenan-induced response compared to a vehicle at 1 h (90%), 2 h (52%), and 4 h (32%) post-carrageenan injection (Figure 7A). Pretreatment with the positive control indomethacin via IP injection (5 mg/kg)

resulted in a significant inhibition of the carrageenan-induced response at 1 h (79%), 2 h (56%), 4 h (54%), and 6 h (48%) post-carrageenan injection (Figure 7A). The obtained inhibitory levels of this COX-inhibitor are in line with previous findings in the rat paw edema model.<sup>40</sup>

Various mediators appear to be involved in the acute inflammation process of the rat paw edema model, including pro-inflammatory cytokines, histamine, 5-hydroxytryptamine (5-HT), prostaglandins, and kinins.<sup>41</sup> It has been described by Di Rosa et al.<sup>42</sup> that carrageenan-induced edema is characterized by an interplay of 3 distinct phases, namely an initial phase mediated by histamine and 5-HT, a second phase regulated by release of kinins, and a third phase where prostaglandins play the main role in the inflammation-dependent edema formation. Kininogen depletion experiments in the rat paw edema model with cellulose sulfate indeed demonstrated that the inhibitory effect on the edema formation was limited to 2.5 h. Therefore, the area under the curve was calculated for the different conditions from 0 to 2 h, which revealed a prominent dose-response for both peptides (Figure 7B). The two higher doses (30 mg/kg and 10 mg/kg) showed significant inhibition of edema formation for both **2d** and **1b** ( $p < 0.05$ ).

**Effect on Retinal Vessel Permeability in Diabetic Rodent Models.** Streptozotocin (STZ) is a glucosamine-nitrosourea sugar analogue selectively toxic to pancreatic beta-cells. Administration of STZ in animal models results in insulin deficiency and systemic hyperglycemia. STZ rodent models are one of the most popular type 1 diabetic models and have been routinely used in fundamental studies and therapeutic drug experiments.<sup>43</sup> Retinal vascular permeability, measured by analyzing extravasation of FITC-BSA (fluorescein isothiocyanate-labeled bovine serum albumin), was markedly increased in mice (3-fold) and rats (1.5-fold) after STZ-induction of diabetes compared to nondiabetic control animals (Figure 8). In the mouse model, a single application of  $6.2 \mu\text{g}/\text{eye}$  of the positive control anti-VEGFR2 antibody DC101 resulted in a pronounced reduction (57%,  $p < 0.05$ ) of the diabetes-dependent retinal permeability 8 weeks after diabetes onset. Similarly, a repeated  $4 \times 100 \mu\text{g}$  IVT administration of peptide **1b** resulted in a statistically significant reduction of the DR-related retinal vascular permeability (36%,  $p < 0.05$ ; Figure 8A). In the same model, treatment with peptide **2d** did not result in a statistically significant reduction of the retinal permeability (data not shown), most probably because of its lower cross-reactivity against the mouse PKal (Table 1). However, peptide **2d** did show efficacy in a diabetic rat STZ model where sufficient cross-reactivity of **2d** against rat PKal is maintained (Table 1). Intravitreal administration of **2d** ( $100 \mu\text{g}/\text{eye}$ ) resulted in a 30% reduction in retinal vascular leakage (back to baseline levels) 4 weeks after diabetes onset, as compared to the vehicle-treated group ( $p < 0.05$ ) (Figure 8B). This effect was comparable to the one obtained with a soluble VEGF-trap positive control (Figure 8B).

## DISCUSSION AND CONCLUSIONS

Constrained peptides, like macrocyclic or bicyclic peptides, allow the conformational locking of the bioactive, productive conformation, resulting in lower entropic cost on binding, consequently leading to dramatically increased affinity and specificity compared to the linear peptides derived from the same sequence.<sup>44–47</sup> Due to their large, extended interaction surface areas, such scaffolds have proven useful to target

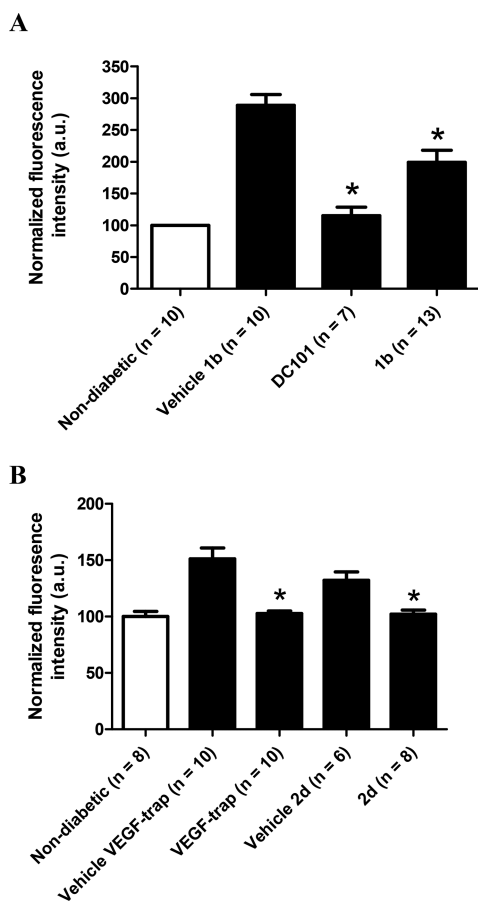


**Figure 8.** (A) Efficacy of peptide **1b** in a diabetic, male C57BL/6J mouse model of retinal permeability. Black bars represent data for diabetic animals. Both treatment with the anti-VEGFR2 positive control antibody DC101 as well as repeated intravitreal injections of **1b** decreased vessel leakage as compared to vehicle-treated diabetic mice. (B) Efficacy of peptide **2d** in a diabetic, male Brown-Norway rat model of retinal permeability. Black bars represent data for diabetic animals. Intravitreal administration of 100  $\mu\text{g}/\text{eye}$  of **2d** resulted in a statistically significant reduction of vascular leakage, as compared to vehicle-treated animals. The effect was comparable to the one obtained following administration of a soluble VEGF-trap used as a positive control. Data are shown as mean  $\pm$  SEM (\*  $p < 0.05$ ).

proteins that otherwise are intractable by typical small molecules.<sup>48–50</sup> Here we describe the generation of human PKal bicyclic peptide inhibitors. The power of phage display-based selections of constrained peptide libraries combined with rationally designed synthetic modifications has allowed the identification of molecules that combine potency, specificity, favorable pharmacokinetics, and *in vivo* stability.

With low nanomolar or subnanomolar  $K_i$  values against human PKal (e.g., 0.15 and 0.36 nM for **2b** and **2d**, respectively), these bicyclic peptides exhibit affinities similar to DX-2930 (reported  $K_i = 0.12$  nM),<sup>40</sup> an anti-PKal antibody currently in Phase 3 for the treatment of patients with type I and type II HAE (ClinicalTrials.gov Identifier: NCT02586805), and, more generally, within the high end of the range of affinities observed for antibodies.<sup>51</sup> Importantly, we also show that these peptides can prevent the release of the bioactive peptide BK both in plasma and in vitreous humor, thereby demonstrating the ability of these molecules to block PKal activity against its natural substrate HMWK. The exquisite target selectivity of **1b** and **2d** (>10,000–100,000 fold

difference in  $K_i$  between PKal and other serine proteases tested) eventually led us to focus our attention on these two peptides.

Achieving good species cross-reactivity beyond cynomolgus monkey proved more challenging, and with the exception of **1b** against the rat enzyme ( $K_i = 3.1$  nM), the latter peptide and **2d** showed either a more limited or a poor degree of cross-reactivity against PKal from other species. Nonetheless, the cross-reactivity toward rat and mouse PKal proved sufficient to demonstrate efficacy in the rat paw edema model with both **1b** and **2d** and in a mouse and rat diabetic eye vessel permeability model with **1b** and **2d**, respectively.

The **1b** and **2d** peptides, even at concentrations of up to 10  $\mu\text{M}$ , induced only a clinically nonrelevant prolongation of the clotting time in the aPTT assay. As PKal is part of an amplification loop in this pathway, this observation is at first sight surprising. Other PKal inhibitors have indeed been reported to more markedly impact the aPTT coagulation time. E.g., KALI-DY, an engineered molecule obtained from Kunitz domain phage libraries, prolonged the aPTT clotting time by more than 3.5-fold at 1  $\mu\text{M}$ ,<sup>33</sup> and PF-04886847, a small molecule competitive inhibitor of PKal, increased the aPTT clotting time 2-fold at 14  $\mu\text{M}$ .<sup>52</sup> However, both KALI-DY and PF-04886847 inhibit Factor XIa at  $K_i = 8.2$  nM and 1  $\mu\text{M}$ , respectively,<sup>33,53</sup> which should amplify their activity in the aPTT assay. It is therefore conceivable that the more limited effect of **1b** and **2d** on the aPTT clotting time is in fact due to their highly specific selectivity profile against other serine proteases from the clotting cascade. This hypothesis is supported by the fact that **4b**, which does show some activity against Factor XIa ( $K_i = 0.5$   $\mu\text{M}$ , Table 4), is able to increase the aPTT clotting time  $\sim$ 1.5-fold at 10  $\mu\text{M}$ .

The *in vivo* stability and pharmacokinetic properties of the peptidic bicyclic inhibitors are essential parameters to consider. Despite their constrained conformation, the peptides are not necessarily stable *in vitro* or *in vivo*, as seen for example for **2b** (Tables 2 and 5). To this end, protease recognition points were removed in **2b** by replacing arginine with homoarginine and by introduction of a nonpeptidic, protease stable  $\text{CH}_2\text{-NH}$  pseudopeptide bond at His<sub>7</sub>. Associated minor losses in affinity due to homoarginine introduction were counteracted by the replacement of proline with the more constrained analogue azetidine carboxylic acid. The resulting derivative **2d** was virtually equipotent to its progenitor **2b** and by contrast highly stable in all tested biological matrices, whether vitreous humor or plasma. **1b** by contrast, although not specifically engineered for proteolytic stability, was natively stable in all matrices tested (Table 2).

*In vivo* plasma clearance in the rat for **1b** and **2d** was consistent with renal clearance at glomerular filtration rate, confirming that unlike the nonstabilized **2b**, **1b** and **2d** are not measurably cleared *in vivo* by other mechanisms, such as proteolytic degradation (Table 5). In the context of drugs developed for ophthalmologic indications, the relatively fast clearance from the circulation is generally seen as an advantage since it limits the risk of systemic toxicity.

By contrast, clearance in the rabbit eye was low, with a half-life of 39 h for **2d**, only  $\sim$ 2–3 times shorter than much larger molecules such as antibodies or antibody fragments.<sup>54,55</sup> With a molecular weight  $\sim$ 90-fold smaller than conventional antibodies, and a similar potency, the slightly faster clearance in the eye can conceivably be compensated by achieving a much

higher molar concentration of the active agent following IVT administration.

Despite a somewhat limited species cross-reactivity, both **1b** and **2d** showed *in vivo* efficacy in a rat paw edema model as good as or superior to the positive control indomethacin. Corresponding to our findings, Kenniston et al. reported a paw edema reduction of 47.2% and 55.6% after pretreatment with indomethacin (5 mg/kg) and DX-2930 (30 mg/kg), respectively.<sup>40</sup>

While significant progress in therapeutic management of diabetic retinopathy has been achieved, it remains the major cause of blindness in industrialized countries. In the past decades, therapies focused on symptomatic prevention of vision loss. In the meantime, the elucidation of the molecular pathways underlying the disease has become the cornerstone of future drug development. IVT administration of anti-VEGF agents has emerged as a primary therapy and is often very effective in reducing macular edema and improving visual acuity.<sup>56</sup> However, frequent injections are needed to achieve full pharmacological benefit, and a significant fraction of the patients responds poorly or is refractory to the therapy. Furthermore, anti-VEGF agents block both the pathological as well as the potential beneficial effects of VEGF in the eye.<sup>57–61</sup> Inhibition of the pathways leading to edema downstream of VEGF or inhibition of VEGF-independent pathways therefore represents attractive therapeutic opportunities.

Recently, Clermont and co-workers<sup>62</sup> showed that PKal, although not involved in the direct effects of VEGF, is required for the full effects of VEGF and other mediators of edema (e.g., TNF- $\alpha$ ) on retinal vascular permeability and retinal thickening, suggesting that PKal contributes to the sustained effects of VEGF and other mediators on blood-retinal barrier function. The authors hypothesized that extravasation of PKal into the retina induced by mediators of edema (including VEGF) contributes to their effects on retinal edema, e.g. by increasing intraocular bradykinin. The same authors, however, demonstrated that PKal is not required for VEGF's angiogenic effects that are critical for vascular growth and survival. In another study, Kita and co-workers<sup>22</sup> reported that the levels of PKal and prekallikrein, on the one hand, and those of VEGF, on the other hand, are elevated in the vitreous of DME patients but do not correlate. Also, the RVP response induced by IVT injection of vitreous from DME patients containing high levels of PKal and low levels of VEGF in diabetic rats was not affected by anti-VEGF or anti-VEGFR2 treatment.<sup>22</sup> Taken together, these results implicate the KKS system as a VEGF-independent mediator of retinal permeability and identify PKal as a promising target for the treatment of diabetes-related eye diseases such as DME.

In conclusion, we describe the identification and design of highly stable, potent, and selective human PKal inhibitory bicyclic peptides and report their prolonged retention in the eye together with *in vivo* efficacy in diabetic models of retinal vascular permeability. Noteworthy, peptide **2d** also proved to be safe upon systemic administration in rat and cynomolgus, with no overt toxicological effect observed at the highest tested systemic dose of 125  $\mu$ g (0.43–0.60 mg/kg) in rat and 1.25 mg (0.42–0.49 mg/kg) in cynomolgus (data not shown). Taken together, these data demonstrate the potential of PKal inhibitory bicyclic peptides for the treatment of diabetes-related eye diseases.

## ■ EXPERIMENTAL SECTION

**Reagents, Enzymes, and Proteins.** Aprotinin was purchased from Sigma-Aldrich (cat. A6279). Single-chain HMWK was obtained from Enzyme Research Laboratories (cat. HK1300) or Creative BioMart (cat. KNG1-1844H). PKal purified from human plasma was purchased from Molecular Innovations (cat. HPAK). Recombinant mouse PKal was from R&D Systems (cat. 2498-SE). Rat PKal was either prepared in-house (see below) or purchased from Athens Research & Technology (cat. 16-16-110112-RAT).

PKal from other species was prepared in-house. Briefly, 250 mL of plasma was mixed with 250 mL of chloroform, and the top (aqueous) phase was collected and activated by addition of an equal volume of a 10 mg/mL suspension of kaolin in H<sub>2</sub>O. The activated plasma phase was then acidified by addition of 500 mL of 1/6 N HCl, incubated at room temperature for 15 min, and neutralized by addition of 500 mL of 1/6 N NaOH. This material was then filtered (0.45  $\mu$ m) and purified in two steps. First, a 12 mL SoyBean Trypsin Inhibitor-agarose (Thermo Scientific, cat. 20235) column was used for the capture of the activated PKal. Following alkaline elution with 10 mM NaOH, the active fractions (see activity assay below) were pooled and pH-adjusted by a 1:1 dilution in 100 mM sodium acetate, pH 5.3. The material was then loaded on a 1 mL Mono S column (GE Healthcare, cat. 17-5168-01) equilibrated with 50 mM sodium acetate, pH 5.5 for polishing and eluted with a 0 to 2 M NaCl gradient on 20 column volumes. The active fractions were pooled and dialyzed against 4 mM sodium acetate, 0.15 M NaCl, pH 5.3 before storage.

The source of the other serine proteases (all of human origin) was as follows: KLK1 (cat. 10407-H08H), KLK6 (cat. 12142-H08H), and KLK13 (cat. 10199-H08H) were from Sino Biological Inc., KLK2 (cat. 4104-SE), KLK5 (cat. 1108-SE), KLK12 (cat. 3095-SE), KLK14 (cat. 2626-SE), Factor Xa (cat. 1063-SE), matriptase (cat. 3946-SE), and complement component C 1s (cat. 2060-SE) were from R&D Systems, alpha thrombin (cat. HT1002A), Factor XIa (cat. HFXIa-2810), Factor XIIa (cat. HFXIIa-2764AL), and Factor VIIa (cat. HFVIIa) were from Enzyme Research Laboratories, granzyme B (cat. BML-SE238) and cathepsin G (cat. BML-SE283) were from Enzo Life Sciences, plasmin (cat. HCPM-0140) was from Haematologic Technologies Inc., and activated protein C (cat. P2200) was from Sigma.

All other reagents were of analytical grade.

### Identification of Plasma Kallikrein Inhibitory Peptides.

Bicyclic peptides (Bicycles) with inhibitory activity against PKal were identified using Bicycle Therapeutics proprietary phage display platform, which is derived from methodology developed by Heinis and Winter.<sup>26</sup> Briefly, linear peptide libraries containing randomized AA between 3 cysteine residues were displayed on the surface of filamentous phage and cyclized on the phage with a thiol-reactive molecular scaffold (TBMB). The libraries formats used were 5  $\times$  5 and 6  $\times$  6, such that either 5 or 6 randomized AA were between the first and second and second and third cysteine, respectively. Following cyclization of the phage libraries, repeated selections were performed against human and rat PKal, according to methodology previously described.<sup>29</sup> Phage clones isolated from the selections were sequenced, and peptides were chemically synthesized for characterization.

**Synthesis and Optimization and of Plasma Kallikrein Inhibitory Peptides.** The synthesis of bicyclic peptides was performed by first synthesizing the linear peptide by standard Fmoc (9-fluorenylmethyloxycarbonyl) solid phase peptide synthesis, using a Symphony automated peptide synthesizer (Protein Technologies) and Rink amide resin. Following cleavage from the resin, peptides were precipitated with diethyl ether, lyophilized, and optionally purified by HPLC (using a Phenomenex Luna C8 or Gemini C18 column) with H<sub>2</sub>O/0.1% (v/v) trifluoroacetic acid (TFA) (A) and acetonitrile/0.1% (v/v) TFA (B) as solvents. Cyclization of the linear peptides (either crude or prepurified) with TBMB was performed in 30–60% (v/v) acetonitrile in water at  $\sim$ 1 mM concentration peptide with  $\sim$ 1.3 equiv TBMB, using ammonium bicarbonate (100 mM) as base. Completion of cyclization was followed by matrix assisted laser desorption ionization time-of-flight (MALDI-TOF) (Voyager DE, Applied

Biosystems), and crude reactions were lyophilized and purified as described above. Eligible fractions containing cyclized peptide of sufficient purity and correct molecular weight (verified again by MALDI-TOF) were pooled, lyophilized, and reconstituted in buffer prior to use. The final purity of the peptides was confirmed at >95% based on UPLC analysis at 215/254 nm using a Waters CSH column (1.7  $\mu\text{m}$   $\times$  2.1 mm  $\times$  150 mm) employing the solvent system described above and a gradient of 5%–30% B in 0–20 min and 30%–55% B in 20–50 min. Key compounds **1b**, **2d**, and **4b** were prepared as the acetate salt (obtained by ion exchange using HPLC and 0.5% acetic acid in place of TFA in the mobile phase, followed by lyophilization), and molecular weights were further verified by LC-MS. Concentrations were estimated by absorption using the extinction coefficient at 280 nm, which was based on Trp/Tyr content. Standard Fmoc AA as well as nonproteinogenic Fmoc-AA were obtained from Sigma-Aldrich and Iris Biotech GmbH. Synthesis of the pseudopeptide bond in **2d** was adapted from protocols reported in Sasaki and Coy, using Fmoc-L-alanine-aldehyde from Bachem.<sup>63</sup> Peptide sequences described here are summarized in Supporting Information Table 1.

**Plasma Stability Profiling.** A rapid plasma stability profiling assay was developed that employed mass spectrometric detection (MALDI-TOF, Voyager DE, Applied Biosystems) of the parent mass and protease-induced metabolites. One millimolar peptide stocks (in DMSO) were diluted into mouse, rat, or human plasma (Seralabs, citrate as anticoagulant) to a concentration of 50  $\mu\text{M}$  and incubated at 37  $^{\circ}\text{C}$  up to 2 days. At various time points, 10  $\mu\text{L}$  of samples was withdrawn, added to 30  $\mu\text{L}$  of 1:1 acetonitrile/methanol, and centrifuged at 13,000 rpm for 5 min. Five microliters of supernatant was withdrawn and mixed with 5  $\mu\text{L}$  of 30 mM ammonium bicarbonate dissolved in 1:1 acetonitrile/water. For mass spectrometric analysis, 1  $\mu\text{L}$  of the mixture was spotted directly onto the MALDI plate. Matrix ( $\alpha$ -cyanocinnamic acid, Sigma, prepared as a saturated solution in 1:1 acetonitrile:water containing 0.1% (v/v) TFA) was layered over the sample (1  $\mu\text{L}$ ) and dried, and total ion chromatograms were obtained for analysis.

**Nonlinear Regression Analyses.** Nonlinear regression analyses were performed using the GraphPad Prism software ver. 5.02 (GraphPad Software Inc., La Jolla, CA), applying, unless otherwise stated, equal weighting (i.e., performing minimization based on absolute distances squared).

**Plasma Kallikrein Activity Measurements.** The hydrolytic activity of PKal was measured using the fluorogenic substrate H-Pro-Phe-Arg-AMC (Bachem, cat. I-1295.0050). Typical substrate concentrations were 10–25  $\mu\text{M}$ . Substrate hydrolysis was monitored by

recording the increase in fluorescence at 480 nm (with excitation at 360 nm) using a Spectramax M2e plate reader (Molecular Devices). The measurements were performed in such a way that no more than 10% of the substrate were hydrolyzed, therefore allowing the determination of initial rates of hydrolysis.

**Enzyme Inhibition Assays and  $K_i$  Measurements.** The intrinsic potency of the bicyclic peptides was determined through  $K_i$  measurements in enzyme inhibition assays. Experiments were performed at 25  $^{\circ}\text{C}$  in 50 mM Tris-HCl, 250 mM NaCl, 1.5  $\mu\text{M}$  bovine serum albumin, pH 7.5. PKal (typical nominal concentration 1–2 nM) was preincubated in 96-well plates with different concentrations of the tested peptide (or of aprotinin, used as a control molecule) for 15 min. The maximum final concentration of a given peptide was chosen based on its potency and was followed by a 1.25- to 3-fold serial dilution, plus a control with no peptide. The reactions were initiated by the addition of H-Pro-Phe-Arg-AMC at a final concentration of 10 to 25  $\mu\text{M}$ , and initial rates of substrate hydrolysis were determined by linear fit of the raw fluorescence versus time traces.

The data were plotted as the initial rate of substrate hydrolysis as a function of the peptide concentration and were fitted to eq 1,<sup>33</sup> where the parameters  $v_0$ ,  $[\text{PKal}]_0$ ,  $[\text{I}]_0$ , and  $K_{i,\text{app}}$  are the rate of substrate hydrolysis in the absence of peptide, the total concentration of PKal, the total concentration of peptide, and the apparent  $K_i$ , respectively. Eq 1 is the full rate equation for a reaction inhibited by a tight-binding inhibitor. It is however applicable to both tight-binding inhibitors ( $K_i < [\text{PKal}]_0$  or  $K_i \sim [\text{PKal}]_0$ ) and poor inhibitors ( $K_i > [\text{PKal}]_0$ ). Here, the term  $[\text{PKal}]_0$  was either treated as an adjustable parameter (potent inhibitors) or fixed to its estimated value (poor inhibitors). The terms  $v_0$  and  $K_{i,\text{app}}$  were always treated as adjustable parameters.

The way the term  $K_{i,\text{app}}$  is linked to the absolute  $K_i$  value depends on the inhibition mechanism. Here, and although not demonstrated experimentally, the blocking peptides were considered to be competitive inhibitors, and therefore eq 2, where  $[\text{S}]$  and  $K_m$  are the substrate concentration and the  $K_m$  of the enzyme for this particular substrate, respectively, applies. Eq 2 shows that the apparent inhibitory potential of a competitive inhibitor decreases with increasing concentrations of substrate. In the case of H-Pro-Phe-Arg-AMC however, the  $K_m$  for PKal is large (not shown), and all experiments were performed under conditions where  $[\text{S}] \ll K_m$ . Therefore,  $K_{i,\text{app}}$  values obtained from eq 1 can be considered as representing actual  $K_i$  values.  $K_i$  values reported are presented as mean  $\pm$  SD. The number of replicate measurements varied between 2 and 60, depending on the compound and the enzyme tested.

$$v_i = v_0 \cdot \left\{ 1 - \frac{([\text{PKal}]_0 + [\text{I}]_0 + K_{i,\text{app}}) - \sqrt{([\text{PKal}]_0 + [\text{I}]_0 + K_{i,\text{app}})^2 - 4 \cdot [\text{PKal}]_0 \cdot [\text{I}]_0}}{2 \cdot [\text{PKal}]_0} \right\} \quad (1)$$

$$K_{i,\text{app}} = K_i \cdot \left( 1 + \frac{[\text{S}]}{K_m} \right) \quad (2)$$

**Specificity Profiling.** A panel of 18 serine proteases of human origin was identified from commercial sources (see above). The synthetic substrates as well as the conditions of the assay were chosen following the providers' recommendations. The peptides were first tested at a concentration of 50  $\mu\text{M}$  for their ability to inhibit the selected proteases. Whenever detectable inhibition was observed, the  $K_i$  of the peptide toward a particular protease was determined by measuring the hydrolytic activity in the presence of various peptide concentrations and analyzing the data with eq 1.

**Activated Partial Thromboplastin Time.** The aPTT clotting times were measured on a BCS-XP coagulation analyzer (Siemens) using actin FS, 0.025 M  $\text{CaCl}_2$ , FVIII-deficient human plasma, and Owren's Veronal Buffer, pH 7.35 (all from Siemens) and were

performed according to the manufacturer's recommendations. Peptide concentration ranged from zero (vehicle control) to 10  $\mu\text{M}$ .

**Inhibition of Bradykinin Release in Plasma.** The peptides were incubated at various concentrations (including a vehicle, i.e. zero concentration, control) in human plasma (Siemens, SMN10446238) for 15 min. The plasma samples were then diluted 2-fold in a 10 mg/mL suspension of kaolin in order to convert endogenous prekallikrein into active Pkal at 37  $^{\circ}\text{C}$ . Bradykinin (BK) generated by the activity of PKal on the endogenous HMWK was then quantified by ELISA (Enzo Life Sciences, cat. ADI-900-206) 15 min after the addition of kaolin. In order to block any further accumulation of BK as well as to stabilize BK, the plasma samples were treated with a cocktail of protease inhibitors (ROCHE, cat. 04693116001) prior to performing the ELISA. The measured BK concentration was plotted as a function of the peptide concentration (in plasma, prior to the addition of kaolin), and the data were fitted to eq 3, where  $[\text{I}]_0$  is the total concentration of peptide, A and D are the BK concentrations in the absence and in the presence of saturating concentrations of peptide, respectively, and B is an empirical fitting parameter, in order to calculate the  $\text{IC}_{50}$  of the

inhibition reaction.  $IC_{50}$  values reported here are expressed as mean  $\pm$  SD of 15 (peptide **2d**) and 6 (peptide **1b**) individual experiments.

$$[BK] = \left( \frac{A - D}{1 + \left( \frac{[I]_0}{IC_{50}} \right)^B} \right) + D \quad (3)$$

**Inhibition of Bradykinin Release in Vitreous.** Pig vitreous was homogenized and clarified as previously described<sup>64</sup> and dialyzed against phosphate buffered saline (PBS) in order to stabilize the pH to physiological values. Human PKal (nominal concentration 10 nM) was incubated in the presence of various concentrations of peptide (including a vehicle, i.e. zero concentration, control) at 37 °C for 15 min in vitreous, at which point purified, single-chain HMWK (final concentration 25  $\mu$ g/mL) was added. After an additional 15 min incubation at 37 °C, the reaction was stopped by the addition of a cocktail of protease inhibitors, and the BK levels were quantified by ELISA as described above. The BK concentration was plotted as a function of the peptide concentration, and the data were fitted to eq 3 to calculate the  $IC_{50}$  of the inhibition reaction.  $IC_{50}$  values reported here are expressed as mean  $\pm$  SD of 3 individual experiments.

#### Measurement of Stability in Plasma and Vitreous Humor.

The half-life of degradation of the peptides in plasma or vitreous was used to assess the comparative stability. Peptide stock solutions in DMSO at 0.16 mM were mixed with plasma (human, rat, or mouse, obtained from Seralabs) or with human vitreous humor (from vitreous biopsies collected by Dr. Joachim Van Calster at the University Hospital Leuven, Belgium) to a final concentration of 4  $\mu$ M and 1  $\mu$ M, respectively. Vitreous was homogenized as described above. The samples (containing an analytical internal standard) were incubated up to 24 h at 37 °C. Forty microliters of plasma samples and 20  $\mu$ L of vitreous samples were collected at various time points and frozen at -80 °C. For analysis, samples were thawed rapidly, and aliquots were treated with 3 volumes of extraction solvent (1:3:3 v/v/v mixture of water, acetonitrile, and methanol). Precipitated proteins were removed by centrifugation (40 min at 13,000 rpm and at 4 °C), and the supernatant was analyzed for the remaining parent peptide by LC-MS/MS (Waters TQD) using standard bioanalytical protocols. Summarizing briefly, two collision-induced fragment ions of each peptide were first quantitated in calibration lines (concentration range 0.25 to 4  $\mu$ M) in the presence of vitreous/plasma (extracted as described above), and the linearity and specificity of the responses were verified (5  $\mu$ L injection onto a Waters BEH C18 column, using a 0.1% formic acid in water/acetonitrile solvent system and 8 min elution gradient of 5 to 60% acetonitrile). Signal to background ratios were >10 at all concentrations. Subsequently, samples derived from the stability time course were quantitated against the calibration line and half-lives estimated by performing nonlinear regression fitting assuming a single exponential decay process.

**Animal Studies.** Housing and all experimental procedures were conducted according to accepted best practice (EU Directive/AAALAC or similar) and approved by Institutional Animal Care and Research Advisory Committee of the KU Leuven, according to the 2010/63/EU Directive. All animal procedures were also performed in accordance with the ARVO Statement for the Use of Animals in Ophthalmic and Vision Research.

**Measurement of Pharmacokinetics Following Intravenous Administration.** Intravenous pharmacokinetics studies were conducted at Argenta Discovery and BioFocus for the *in-life* and *in vitro* aspects, respectively. Groups of 2 male Sprague-Dawley rats were administered 5 mg/kg of **2d** or **1b**. In a separate experiment, **2b** was administered as an infusion into the jugular vein of 10 mg/kg peptide over 1 h. Serial blood samples were taken from each animal via temporary indwelling tail vein cannulae at 5, 10, 20, 30, 60, 120, 180, and 240 min postdose, into EDTA tubes, and centrifuged to generate plasma samples for analysis.

Peptide concentration in plasma samples was quantified by LC-MS/MS as detailed above, using calibration lines at concentrations between 16 and 4000 ng/mL in control rat plasma, 5  $\mu$ L sample injections with

a 0.01% formic acid in water/acetonitrile solvent system, and a 1 min elution gradient of 5 to 95% acetonitrile. The limits of quantification for **1b** and **2d** were 16 and 32 ng/mL, respectively. For peptides **2d** and **1b**, pharmacokinetic parameters were determined by non-compartmental analysis using PK Solutions 2.0 (Summit Research Services). Area under the curve values were calculated by the trapezoidal method.

**Measurement of Pharmacokinetics Following Intravitreal Administration.** For IVT studies, male New-Zealand White rabbits (10 weeks old, ~2 kg, Charles River) received a single injection of 50  $\mu$ L of **2d** (2 mg/mL in 50 mM sodium phosphate, pH 7.2) in each eye. IVT injections were performed using a 30G insulin needle of 0.3 mL with half-unit (50  $\mu$ L) marks. The animals were sacrificed 15 min, 1 h, 4 h, 8 h, 24 h, 48, and 96 h after injection (3 animals per time point), the injected eyes were enucleated, and the complete vitreous was collected. The vitreous samples were homogenized and clarified as described above and then further clarified by 0.2  $\mu$ m filtration (Nanosep MF with Bio-Inert membrane, WVR). The peptide was then quantified in the vitreous samples by HPLC using an Acquity UPLC instrument (Waters). Samples were diluted with 1.5 volumes of 8.33% (v/v) acetonitrile, 0.17% (v/v) TFA, 0.067% (v/v) Tween-20, and 6  $\mu$ L was injected on a BEH300 C18 1.7  $\mu$ m, 2.1  $\times$  100 mm Acquity UPLC column. Elution was performed over 10 min (0.1 mL/min) from 5 to 40% acetonitrile in the presence of 0.1% TFA, monitoring at 215 nm. The concentration of peptide in the samples was calculated by integration of the relevant peak and reference to a standard curve obtained under conditions of linear response.

The peptide concentration was plotted as a function of the time of collection, and the half-life in the eye (reported as best-fit value  $\pm$  standard error) was obtained by fitting the data with eq 4, where  $C_0$  and HL are the peptide concentration at time zero and the half-life in the eye, respectively, using a proportional weighting.

$$C = C_0 \cdot e^{-\frac{\ln 2}{HL} t} \quad (4)$$

**Rat Model of Carrageenan-Induced Paw Edema.** The rat paw edema model study was performed by Washington Biotechnology, Inc. Male Sprague-Dawley rats with a body weight of 180–200 g (~6–7 weeks old) (Harlan Laboratories) were randomized into 8 experimental groups ( $n = 10$ ). The animals received one IP injection of either formulation buffer (vehicle: 20% PEG 400, 10% Kolliphor, 50 mM sodium acetate, pH 5), indomethacin positive control (Sigma, 5 mg/kg prepared in 0.1 M NaHCO<sub>3</sub> at a concentration of 1.25 mg/mL), or different doses of either **2d** or **1b** (3, 10, or 30 mg/kg prepared in 20% PEG 400, 10% Kolliphor, 50 mM sodium acetate, pH 5, at concentrations of 7.5, 2.5, and 0.75 mg/mL, respectively). The dose range for **2d** and **1b** was similar to the one used with DX-2930 in the same model.<sup>40</sup> Fifteen minutes after treatment, the rats were injected subcutaneously into the subplantar region of the right hind paw with 0.1 mL of 1% lambda carrageenan (Fluka, prepared in deionized water). Right hind paw volumes were recorded by means of plethysmography before and 1, 2, 4, and 6 h after carrageenan injection. Results or measurements are reported to be significantly different for probability values ( $p$ -values) < 0.05.

**Diabetic Rodent Models of Retinal Permeability.** Male C57BL/6J mice (3–5 weeks old) and male Brown-Norway rats (200–250 g, 9 weeks old) were obtained from Charles River Laboratories (L'Arbresle Cedex, France). Mice were rendered diabetic with 5 consecutive daily IP injections of STZ (Sigma-Aldrich, cat. S0130) at 50 mg/kg freshly dissolved in 100 mM sodium citrate, pH 4.5, whereas rats received a single IP injection of 55 mg/kg STZ (dissolved in the same buffer). Animals treated IP with the vehicle served as nondiabetic controls ( $n = 10$  for mice, and  $n = 8$  for rats). Blood glucose levels were monitored weekly after the first STZ injection (glucometer, OneTouch Vita, LifeScan Inc., Milpitas, CA, USA), and diabetic status was defined by glucose levels higher than 250 mg/dL. Only animals with consistent hyperglycemic levels were included in the experimental diabetic groups. No exogenous insulin treatment was given.

Seven weeks after diabetes onset, the first two diabetic mice groups were treated with four binocular IVT injections of **1b** (100  $\mu\text{g}/\text{eye}$ , using a 100 mg/mL solution of the peptide prepared in 15 mM NaOH in water, with pH adjusted to 5.4–5.5 with acetic acid;  $n = 13$ ) or vehicle ( $n = 10$ ), with an interval of 2 days between each injection. The dosing regimen of **1b** corresponded to the maximal possible dose to compensate for the fast clearance that is expected in rodent eyes. As a positive control, an additional group was treated with one IVT injection of the anti-mouse VEGFR2 antibody DC101 (Thrombogenics N.V. 6.2  $\mu\text{g}/\text{eye}$ , prepared in PBS;  $n = 7$ ). Mice were sacrificed 1 week after initiation of treatment to evaluate vessel leakage. In diabetic rats, peptide **2d** (20 mg/mL in 10 mM HCl;  $n = 8$ ) or vehicle ( $n = 6$ ) was administered IVT immediately after diabetes onset. Here too, dosing of **2d** was maximized to compensate for the fast ocular clearance. As a positive control for the model, an additional group ( $n = 10$ ) with repeated IP injections (3 times a week) of 2 mg/kg of a soluble VEGF-trap (formulated in 10 mM sodium phosphate, 40 mM NaCl, 0.03% Tween-20, 5% sucrose, pH 6.2) was included and compared to its vehicle ( $n = 10$ ). The soluble VEGF-trap used here was a research reagent obtained by recombinant expression of a protein which sequence was identical to the one of aflibercept.<sup>65</sup> Systemic administration was chosen in correlation with previously reported studies in this model.<sup>66,67</sup> Rats were sacrificed 4 weeks after diabetes onset to quantify vascular retinal leakage. The IVT injections in all animals were performed by using an analytic science syringe (SGE Analytic Science) and glass capillaries with a diameter of 50–70  $\mu\text{m}$  at the end, controlled by the UMP3I Microsyringe Injector and Micro4 Controller (all from World Precision Instruments Inc., Hertfordshire, UK).

Retinal permeability was assessed using an approach adapted from previous studies.<sup>68–71</sup> Briefly, FITC-BSA (Sigma-Aldrich, cat. A9771) dissolved in PBS (10 mg/mL) was injected retrobulbarly in the right eye (OD) in mice (at 100  $\mu\text{g}/\text{g}$ ) and via vena femoralis (at 500  $\mu\text{g}/\text{g}$ ) in rats. Twenty to 30 min later, the animals were sacrificed, and eyes were enucleated and placed in 1% formaldehyde overnight followed by paraffin wax embedding. Sagittal serial sections of the left eyes (OS) through the central retina were collected and dewaxed for vessel leakage assessment. Using a fluorescence microscope equipped with a digital camera (Axiocam MrC5, Zeiss), images were taken at a magnification of 20X from retinal cross sections adjacent to either side of the optic nerve head. The retinal fluorescence intensity per image was measured and normalized to the background fluorescence intensity on the slide. Morphometric analyses were performed using a commercial software (KS300 and AxioVision, Zeiss). Results or measurements are reported to be significantly different for  $p$ -values < 0.05.

## ■ ASSOCIATED CONTENT

### ● Supporting Information

The Supporting Information is available free of charge on the ACS Publications website at DOI: 10.1021/acs.jmedchem.7b01625.

Figure of comparative plasma stability of **2b** and **2d**, table of bicyclic peptide names and their corresponding sequences (PDF)

Molecular formula strings (CSV)

## ■ AUTHOR INFORMATION

### Corresponding Author

\*Phone: +32 16 751 340. E-mail: [jean.feyen@thrombogenics.com](mailto:jean.feyen@thrombogenics.com).

### ORCID

Marc Vanhove: 0000-0003-4144-7688

### Present Addresses

#Innate Pharma SA, 117 Avenue de Luminy - BP 30191, 13276 MARSEILLE Cedex 09, France.

<sup>§</sup>Laboratory of Ophthalmology, KU Leuven, Herestraat 49, 3000 Leuven, Belgium.

## Notes

The authors declare the following competing financial interest(s): D.P.T., G.B., H.H., K.v.R., and S.P. are employees at Bicycle Therapeutics Inc.; T.V.B., E.V., P.B., T.-T.H., M.V., and J.H.M.F. work for ThromboGenics N.V.

## ■ ACKNOWLEDGMENTS

The authors wish to thank Prof. Marc Hoylaerts (Department of Cardiovascular Sciences, Center for Molecular and Vascular Biology, University of Leuven, Belgium) for performing the aPTT measurements and Dr. Joachim Van Calster (University Hospital Leuven, Belgium) for providing human vitreous biopsies. The authors also thank Bernard Noppen, Kelly Vanhulst, Huberte Moreau, Astrid De Vriese, Valerie Vanheukelom, Tom Janssens, Sarah Nauwelaerts, Sofie Beckers, Ann Verbeek, and Martine Leijssen for excellent technical support.

## ■ ABBREVIATIONS USED

PKal, plasma kallikrein; CAS, contact activation system; KKS, kallikrein-kinin system; BK, bradykinin; HMWK, high molecular weight kininogen; C1-INH, C1 inhibitor; HAE, hereditary angioedema; DR, diabetic retinopathy; NPDR, nonproliferative diabetic retinopathy; PDR, proliferative diabetic retinopathy; DME, diabetic macular edema; RVP, retinal vascular permeability; TBMB, 1,3,5-tris(bromomethyl)benzene; AA, amino acid; aPTT, activated partial thromboplastin time; IVT, intravitreal; IP, intraperitoneal; 5-HT, 5-hydroxytryptamine; STZ, streptozotocine; FITC-BSA, fluorescein isothiocyanate-labeled bovine serum albumin; TFA, trifluoroacetic acid; SD, standard deviation; SEM, standard error of the mean

## ■ REFERENCES

- (1) Hermann, A.; Arnhold, M.; Kresse, H.; Neth, P.; Fink, E. Expression of plasma prekallikrein mRNA in human nonhepatic tissues and cell lineages suggests special local functions of the enzyme. *Biol. Chem.* **1999**, *380*, 1097–1102.
- (2) Selvarajan, S.; Lund, L. R.; Takeuchi, T.; Craik, C. S.; Werb, Z. A plasma kallikrein-dependent plasminogen cascade required for adipocyte differentiation. *Nat. Cell Biol.* **2001**, *3*, 267–275.
- (3) Leeb-Lundberg, L. M.; Marceau, F.; Müller-Esterl, W.; Pettibone, D. J.; Zuraw, B. L. International union of pharmacology. XLV. Classification of the kinin receptor family: from molecular mechanisms to pathophysiological consequences. *Pharmacol. Rev.* **2005**, *57*, 27–77.
- (4) Schmaier, A. H. The contact activation and kallikrein/kinin systems: pathophysiologic and physiologic activities. *J. Thromb. Haemostasis* **2016**, *14*, 28–39.
- (5) Cochrane, C. G.; Revak, S. D.; Wuepper, K. D. Activation of Hageman factor in solid and fluid phases. A critical role of kallikrein. *J. Exp. Med.* **1973**, *138*, 1564–1583.
- (6) Shariat-Madar, Z.; Mahdi, F.; Schmaier, A. H. Identification and characterization of prolylcarboxypeptidase as an endothelial cell prekallikrein activator. *J. Biol. Chem.* **2002**, *277*, 17962–17969.
- (7) Bork, K.; Meng, G.; Staubach, P.; Hardt, J. Hereditary angioedema: new findings concerning symptoms, affected organs, and course. *Am. J. Med.* **2006**, *119*, 267–274.
- (8) Zanichelli, A.; Mansi, M.; Periti, G.; Cicardi, M. Therapeutic management of hereditary angioedema due to C1 inhibitor deficiency. *Expert Rev. Clin. Immunol.* **2013**, *9*, 477–488.
- (9) Wu, M. A.; Zanichelli, A.; Mansi, M.; Cicardi, M. Current treatment options for hereditary angioedema due to C1 inhibitor deficiency. *Expert Opin. Pharmacother.* **2016**, *17*, 27–40.

- (10) Moss, S. E.; Klein, R.; Klein, B. E. The 14-year incidence of visual loss in a diabetic population. *Ophthalmology* **1998**, *105*, 998–1003.
- (11) Koblin Klein, B. E. Overview of epidemiologic studies of diabetic retinopathy. *Ophthalmic Epidemiol.* **2007**, *14*, 179–183.
- (12) Cheung, N.; Mitchell, P.; Wong, T. Y. Diabetic retinopathy. *Lancet* **2010**, *376*, 124–136.
- (13) Prokofyeva, E.; Zrenner, E. Epidemiology of major eye diseases leading to blindness in Europe: A literature review. *Ophthalmic Res.* **2012**, *47*, 171–188.
- (14) Tolentino, M. S.; Tolentino, A. J.; Tolentino, M. J. Current and investigational drugs for the treatment of diabetic retinopathy. *Expert Opin. Invest. Drugs* **2016**, *25*, 1011–1022.
- (15) Shaw, J. E.; Sicree, R. A.; Zimmet, P. Z. Global estimates of the prevalence of diabetes for 2010 and 2030. *Diabetes Res. Clin. Pract.* **2010**, *87*, 4–14.
- (16) Ting, D. S.; Cheung, G. C.; Wong, T. Y. Diabetic retinopathy: global prevalence, major risk factors, screening practices and public health challenges: a review. *Clin. Experiment. Ophthalmol.* **2016**, *44*, 260–277.
- (17) Mathew, C.; Yunirakasiwi, A.; Sanjay, S. Updates in the management of diabetic macular edema. *J. Diabetes Res.* **2015**, *2015*, 794036.
- (18) Feener, E. P. Plasma kallikrein and diabetic macular edema. *Curr. Diabetes Rep.* **2010**, *10*, 270–275.
- (19) Abdouh, M.; Talbot, S.; Couture, R.; Hasséssian, H. M. Retinal plasma extravasation in streptozotocin-diabetic rats mediated by kinin B(1) and B(2) receptors. *Br. J. Pharmacol.* **2008**, *154*, 136–143.
- (20) Gao, B. B.; Clermont, A.; Rook, S.; Fonda, S. J.; Srinivasan, V. J.; Wojtkowski, M.; Fujimoto, J. G.; Avery, R. L.; Arrigg, P. G.; Bursell, S. E.; Aiello, L. P.; Feener, E. P. Extracellular carbonic anhydrase mediates hemorrhagic retinal and cerebral vascular permeability through prekallikrein activation. *Nat. Med.* **2007**, *13*, 181–188.
- (21) Gao, B. B.; Chen, X.; Timothy, N.; Aiello, L. P.; Feener, E. P. Characterization of the vitreous proteome in diabetes without diabetic retinopathy and diabetes with proliferative diabetic retinopathy. *J. Proteome Res.* **2008**, *7*, 2516–2525.
- (22) Kita, T.; Clermont, A. C.; Murugesan, N.; Zhou, Q.; Fujisawa, K.; Ishibashi, T.; Aiello, L. P.; Feener, E. P. Plasma kallikrein-kinin system as a VEGF-independent mediator of diabetic macular edema. *Diabetes* **2015**, *64*, 3588–3599.
- (23) Clermont, A.; Chilcote, T. J.; Kita, T.; Liu, J.; Riva, P.; Sinha, S.; Feener, E. P. Plasma kallikrein mediates retinal vascular dysfunction and induces retinal thickening in diabetic rats. *Diabetes* **2011**, *60*, 1590–1598.
- (24) Lawson, S. R.; Gabra, B. H.; Guérin, B.; Neugebauer, W.; Nantel, F.; Battistini, B.; Sirois, P. Enhanced dermal and retinal vascular permeability in streptozotocin-induced type 1 diabetes in Wistar rats: blockade with a selective bradykinin B1 receptor antagonist. *Regul. Pept.* **2005**, *124*, 221–224.
- (25) Pouliot, M.; Talbot, S.; Sénécal, J.; Dotigny, F.; Vaucher, E.; Couture, R. Ocular application of the kinin B1 receptor antagonist LF22–0542 inhibits retinal inflammation and oxidative stress in streptozotocin-diabetic rats. *PLoS One* **2012**, *7*, e33864.
- (26) Heinis, C.; Rutherford, T.; Freund, S.; Winter, G. Phage-encoded combinatorial chemical libraries based on bicyclic peptides. *Nat. Chem. Biol.* **2009**, *5*, 502–507.
- (27) Middendorp, S. J.; Willbs, J.; Quarroz, C.; Calzavarini, S.; Angelillo-Scherrer, A.; Heinis, C. Peptide macrocycle inhibitor of coagulation factor XII with subnanomolar affinity and high target selectivity. *J. Med. Chem.* **2017**, *60*, 1151–1158.
- (28) Chen, S.; Bertoldo, D.; Angelini, A.; Pojer, F.; Heinis, C. Peptide ligands stabilized by small molecules. *Angew. Chem., Int. Ed.* **2014**, *53*, 1602–1606.
- (29) Baeriswyl, V.; Rapley, H.; Pollaro, L.; Stace, C.; Teufel, D.; Walker, E.; Chen, S.; Winter, G.; Tite, J.; Heinis, C. Bicyclic peptides with optimized ring size inhibit human plasma kallikrein and its orthologues while sparing paralogous proteases. *ChemMedChem* **2012**, *7*, 1173–1176.
- (30) Teufel, D. P.; Johnson, C. M.; Lum, J. K.; Neuweiler, H. Backbone-driven collapse in unfolded protein chains. *J. Mol. Biol.* **2011**, *409*, 250–262.
- (31) Tugyi, R.; Uray, K.; Iván, D.; Fellingner, E.; Perkins, A.; Hudecz, F. Partial D-amino acid substitution: Improved enzymatic stability and preserved Ab recognition of a MUC2 epitope peptide. *Proc. Natl. Acad. Sci. U. S. A.* **2005**, *102*, 413–418.
- (32) Mahdy, A. M.; Webster, N. R. Perioperative systemic haemostatic agents. *Br. J. Anaesth.* **2004**, *93*, 842–858.
- (33) Dennis, M. S.; Herzka, A.; Lazarus, R. A. Potent and selective Kunitz domain inhibitors of plasma kallikrein designed by phage display. *J. Biol. Chem.* **1995**, *270*, 25411–25417.
- (34) Wu, Y. Contact pathway of coagulation and inflammation. *Thromb. J.* **2015**, *13*, 17.
- (35) Raber, M. N. Coagulation Tests. In *Clinical Methods: The History, Physical, and Laboratory Examinations*, 3rd ed.; Walker, H. K., Hall, W. D., Hurst, J. W., Eds.; Butterworths: Boston, 1990.
- (36) Ruttman, T. Coagulation for the clinician. *S. Afr. J. Surg.* **2006**, *44* (22), 24–26 28–30, 32–37.
- (37) Sebag, J. The vitreous. In *Adler's Physiology of the Eye*; Hart, W., Eds.; Mosby: St. Louis, 1992; pp 268–347.
- (38) Jobin, J.; Bonjour, J. P. Measurement of glomerular filtration rate in conscious unrestrained rats with inulin infused by implanted osmotic pumps. *Am. J. Physiol.* **1985**, *248*, F734–F738.
- (39) del Amo, E. M.; Urtti, A. Rabbit as an animal model for intravitreal pharmacokinetics: clinical predictability and quality of published data. *Exp. Eye Res.* **2015**, *137*, 111–124.
- (40) Kenniston, J. A.; Faucette, R. R.; Martik, D.; Comeau, S. R.; Lindberg, A. P.; Kopacz, K. J.; Conley, G. P.; Chen, J.; Viswanathan, M.; Kastrapeli, N.; Cosic, J.; Mason, S.; DiLeo, M.; Abendroth, J.; Kuzmic, P.; Ladner, R. C.; Edwards, T. E.; TenHoor, C.; Adelman, B. A.; Nixon, A. E.; Sexton, D. J. Inhibition of plasma kallikrein by a highly specific active site blocking antibody. *J. Biol. Chem.* **2014**, *289*, 23596–235608.
- (41) Morris, C. J. Carrageenan-induced paw edema in the rat and mouse. *Methods Mol. Biol.* **2003**, *225*, 115–121.
- (42) Di Rosa, M.; Giroud, J. P.; Willoughby, D. A. Studies on the mediators of the acute inflammatory response induced in rats in different sites by carrageenan and turpentine. *J. Pathol.* **1971**, *104*, 15–29.
- (43) Lai, A. K.; Lo, A. C. Animal models of diabetic retinopathy: summary and comparison. *J. Diabetes Res.* **2013**, *2013*, 106594.
- (44) Mas-Moruno, C.; Rechenmacher, F.; Kessler, H. Cilengitide: the first anti-angiogenic small molecule drug candidate design, synthesis and clinical evaluation. *Anti-Cancer Agents Med. Chem.* **2010**, *10*, 753–768.
- (45) Bock, J. E.; Gavenonis, J.; Kritzer, J. A. Getting in shape: controlling peptide bioactivity and bioavailability using conformational constraints. *ACS Chem. Biol.* **2013**, *8*, 488–499.
- (46) Hill, T. A.; Shepherd, N. E.; Diness, F.; Fairlie, D. P. Constraining cyclic peptides to mimic protein structure motifs. *Angew. Chem., Int. Ed.* **2014**, *53*, 13020–13041.
- (47) Pelay-Gimeno, M.; Glas, A.; Koch, O.; Grossmann, T. N. Structure-based design of inhibitors of protein-protein interactions: mimicking peptide binding epitopes. *Angew. Chem., Int. Ed.* **2015**, *54*, 8896–8927.
- (48) Moellering, R. E.; Cornejo, M.; Davis, T. N.; Del Bianco, C.; Aster, J. C.; Blacklow, S. C.; Kung, A. L.; Gilliland, D. G.; Verdine, G. L.; Bradner, J. E. Direct inhibition of the NOTCH transcription factor complex. *Nature* **2009**, *462*, 182–188.
- (49) Giordanetto, F.; Kihlberg, J. Macrocyclic drugs and clinical candidates: what can medicinal chemists learn from their properties? *J. Med. Chem.* **2014**, *57*, 278–295.
- (50) Upadhyaya, P.; Qian, Z.; Selner, N. G.; Clippinger, S. R.; Wu, Z.; Briesewitz, R.; Pei, D. Inhibition of Ras signaling by blocking Ras-effector interactions with cyclic peptides. *Angew. Chem., Int. Ed.* **2015**, *54*, 7602–7606.
- (51) Frenzel, A.; Roskos, L.; Klakamp, S.; Liang, M.; Arends, R.; Green, L. Antibody Affinity. In *Handbook of Therapeutic Antibodies*;

Dübel, S.; Reichert, J. M., Eds.; Wiley-VCH Verlag GmbH & Co. KGaA: Weinheim, Germany, 2014; DOI: [10.1002/9783527682423.ch6](https://doi.org/10.1002/9783527682423.ch6).

(52) Kolte, D.; Bryant, J. W.; Gibson, G. W.; Wang, J.; Shariat-Madar, Z. PF-04886847 (an inhibitor of plasma kallikrein) attenuates inflammatory mediators and activation of blood coagulation in rat model of lipopolysaccharide (LPS)-induced sepsis. *Cardiovasc. Hematol. Agents Med. Chem.* **2012**, *10*, 154–166.

(53) Kolte, D.; Bryant, J.; Holsworth, D.; Wang, J.; Akbari, P.; Gibson, G.; Shariat-Madar, Z. Biochemical characterization of a novel high-affinity and specific plasma kallikrein inhibitor. *Br. J. Pharmacol.* **2011**, *162*, 1639–1649.

(54) Bakri, S. J.; Snyder, M. R.; Reid, J. M.; Pulido, J. S.; Singh, R. J. Pharmacokinetics of intravitreal bevacizumab (Avastin). *Ophthalmology* **2007**, *114*, 855–859.

(55) Bakri, S. J.; Snyder, M. R.; Reid, J. M.; Pulido, J. S.; Ezzat, M. K.; Singh, R. J. Pharmacokinetics of intravitreal ranibizumab (Lucentis). *Ophthalmology* **2007**, *114*, 2179–2182.

(56) Wells, J. A.; Glassman, A. R.; Ayala, A. R.; Jampol, L. M.; Aiello, L. P.; Antoszyk, A. N.; Arnold-Bush, B.; Baker, C. W.; Bressler, N. M.; Browning, D. J.; Elman, M. J.; Ferris, F. L.; Friedman, S. M.; Melia, M.; Pieramici, D. J.; Sun, J. K.; Beck, R. W. Aflibercept, bevacizumab, or ranibizumab for diabetic macular edema. *N. Engl. J. Med.* **2015**, *372*, 1193–1203.

(57) Saint-Geniez, M.; Maharaj, A. S.; Walshe, T. E.; Tucker, B. A.; Sekiyama, E.; Kurihara, T.; Darland, D. C.; Young, M. J.; D'Amore, P. A. Endogenous VEGF is required for visual function: evidence for a survival role on muller cells and photoreceptors. *PLoS One* **2008**, *3*, e3554.

(58) Saint-Geniez, M.; Kurihara, T.; Sekiyama, E.; Maldonado, A. E.; D'Amore, P. A. An essential role for RPE-derived soluble VEGF in the maintenance of the choriocapillaris. *Proc. Natl. Acad. Sci. U. S. A.* **2009**, *106*, 18751–18756.

(59) Kurihara, T.; Westenskow, P. D.; Bravo, S.; Aguilar, E.; Friedlander, M. Targeted deletion of Vegfa in adult mice induces vision loss. *J. Clin. Invest.* **2012**, *122*, 4213–4217.

(60) Park, H. Y.; Kim, J. H.; Park, C. K. Neuronal cell death in the inner retina and the influence of vascular endothelial growth factor inhibition in a diabetic rat model. *Am. J. Pathol.* **2014**, *184*, 1752–1762.

(61) Domigan, C. K.; Warren, C. M.; Antanesian, V.; Happel, K.; Ziyad, S.; Lee, S.; Krall, A.; Duan, L.; Torres-Collado, A. X.; Castellani, L. W.; Elashoff, D.; Christofk, H. R.; van der Bliek, A. M.; Potente, M.; Iruela-Arispe, M. L. Autocrine VEGF maintains endothelial survival through regulation of metabolism and autophagy. *J. Cell Sci.* **2015**, *128*, 2236–2248.

(62) Clermont, A.; Murugesan, N.; Zhou, Q.; Kita, T.; Robson, P. A.; Rushbrooke, L. J.; Evans, D. M.; Aiello, L. P.; Feener, E. P. Plasma kallikrein mediates vascular endothelial growth factor-induced retinal dysfunction and thickening. *Invest. Ophthalmol. Visual Sci.* **2016**, *57*, 2390–2399.

(63) Sasaki, Y.; Coy, D. H. Solid phase synthesis of peptides containing the CH<sub>2</sub>NH peptide bond isostere. *Peptides* **1987**, *8*, 119–121.

(64) Aerts, F.; Noppen, B.; Fonteyn, L.; Derua, R.; Waelkens, E.; de Smet, M. D.; Vanhove, M. Mechanism of inactivation of ocriplasmin in porcine vitreous. *Biophys. Chem.* **2012**, *165–166*, 30–38.

(65) Stewart, M. W. Aflibercept (VEGF Trap-eye): the newest anti-VEGF drug. *Br. J. Ophthalmol.* **2012**, *96*, 1157–1158.

(66) Qaum, T.; Xu, Q.; Jousen, A. M.; Clemens, M. W.; Qin, W.; Miyamoto, K.; Hassessian, H.; Wiegand, S. J.; Rudge, J.; Yancopoulos, G. D.; Adamis, A. P. VEGF-initiated blood-retinal barrier breakdown in early diabetes. *Invest. Ophthalmol. Vis. Sci.* **2001**, *42*, 2408–2413.

(67) Cao, J.; Song, H.; Renard, R. A.; Liu, Y.; Yancopoulos, G. D.; Wiegand, S. J. Systemic administration of VEGF trap suppresses vascular leak and leukostasis in the retinas of diabetic rats. *Invest. Ophthalmol. Vis. Sci.* **2005**, *46*, 446.

(68) Antonetti, D. A.; Barber, A. J.; Khin, S.; Lieth, E.; Tarbell, J. M.; Gardner, T. W. Vascular permeability in experimental diabetes is

associated with reduced endothelial occludin content: vascular endothelial growth factor decreases occludin in retinal endothelial cells. Penn State Retina Research Group. *Diabetes* **1998**, *47*, 1953–1959.

(69) Kim, J. H.; Kim, J. H.; Jun, H. O.; Yu, Y. S.; Kim, K. W. Inhibition of protein kinase C delta attenuates blood-retinal barrier breakdown in diabetic retinopathy. *Am. J. Pathol.* **2010**, *176*, 1517–1524.

(70) Kim, Y. H.; Kim, Y. S.; Roh, G. S.; Choi, W. S.; Cho, G. J. Resveratrol blocks diabetes-induced early vascular lesions and vascular endothelial growth factor induction in mouse retinas. *Acta Ophthalmol.* **2012**, *90*, e31–e37.

(71) Hollanders, K.; Van Hove, I.; Sergeys, J.; Bergen, T. V.; Lefevre, E.; Kindt, N.; Castermans, K.; Vandewalle, E.; van Pelt, J.; Moons, L.; Stalmans, I. AMA0428, a potent rock inhibitor, attenuates early and late experimental diabetic retinopathy. *Curr. Eye Res.* **2017**, *42*, 260–272.